RESEARCH ARTICLE

Geometry and vertical extent of the late Weichselian ice sheet in northwestern Oppland County, Norway

Bjørn Follestad* **& Ola Fredin**

Geological Survey of Norway, P.O.Box 6315 Sluppen, 7491 Trondheim, Norway.
** bjorn.follestad@ngu.no*

The position of the ice margin during the last deglaciation is well known in Scandinavia, in particular during the Younger Dryas (YD) chronozone from when large ice marginal deposits easily can be traced at or close to the Norwegian coast. However, inland of the YD marginal deposits, the vertical extent and geometry of the Scandinavian ice sheet is still debated. In this study we have used detailed Quaternary geological mapping to reconstruct the ice sheet surface and slope in core areas around the valleys of Gudbrandsdalen, Romsdalen, Eikesdalen/Litledalen and around lake Aursjøen. In these areas we typically find morphologically distinct lateral moraines at 1300–1500 m a.s.l., which slope down towards the coast and seem to correlate with two known YD stages. By using slope and spatial pattern of the lateral moraines we infer a maximum elevation of the YD ice sheet in central areas around Dombås to be at around 2000 m a.s.l., and mostly lower at 1800 m.a.sl. during significant portions of the YD chronozone. Most inland areas in Norway were thus ice covered during YD, except for high peaks in for example Dovre, Rondane and Jotunheimen, which acted as accumulation area nunataks. Our data also show that the first order ice divide during this stage was situated over Jotunheimen from where significant ice streams emanated and were flowing down into the major valleys and out towards the coast. We stress that this study is preliminary, lacking absolute dates of the lateral moraine zones, but the spatial pattern is very consistent and correlates well with known glacial stages. A dating campaign is underway to elucidate the precise timing of these glacial events, but the picture emerging from this work shows the importance of careful Quaternary geological mapping to understand past ice-sheet configurations.

Follestad, B. and Fredin, O. (2011) Geometry and vertical extent of the late Weichselian ice sheet in northwestern Oppland County, Norway. *Norges geologiske undersøkelse Bulletin*, **451**, 1–19.

Introduction

The geometry and vertical extent of the Upper (late) Weichselian Scandinavian ice sheet has been debated and different models have been proposed (e.g., Vorren 1977, Andersen, 1981, 2000, Bergersen and Garnes 1983, Boulton et al. 1985, Nesje et al. 1988, Dahl et al. 1997, Andersen et al. 1995). The different models can be grouped in two classes: the 'thick-ice models' and the 'thin-ice models'—see for example discussions in Dahl et al. (1997), Kleman and Hättestrand (1999), Mangerud (2004) and Paus et al. (2006). These models contrast in the reconstructions of the ice thickness in central Norway. In the maximum models it is suggested that a massive central ice dome existed and covered the landscape completely in central Norway during the late Weichselian glaciation (Andersen et al. 1995, Andersen 2000, Mangerud 2004). The thickness of the ice is considered to have been several thousand metres, and much of the terrain was probably ice covered. In contrast, the minimum glaciations model suggests thinner ice, several local ice domes, and nunataks in core areas (e.g., Nesje et al. 1988) with an ice surface as low as 1100 m a.s.l. in the interior areas of Norway at an early late-glacial interval (Dahl et al. 1997, Paus et al. 2006). In this case, large mountain areas in central Norway and in the Østerdalen valley and Gudbrandsdalen valley are thought to be almost ice free in the late Weichselian.

Based on the data collected through the Quaternary mapping program of the Geological Survey of Norway, the exact vertical extent of a Younger Dryas (YD) glacier surface is established based on the distribution of ice marginal moraines and meltwater channels. This ice surface will be discussed in relation to the existing models for the vertical extent of the late Weichselian Scandinavian ice sheet in central Norway.

General physiographic setting

The investigated area is located in the northwestern part of Oppland County and in the eastern part of Møre and Romsdal County (Figure 1) and is dominated by a landmass reaching 1200–2000 m a.s.l. Tectonic uplift during the Neogene (Ebbing and Olesen 2005) successively heaved the distinct upland plateaus, and the valley of Gudbrandsdalen and tributary valleys were formed by river incision prior to the Quaternary glaciation, as described by Bonow et al. (2003). Through the Quaternary, glaciers inundated this area several times. Glacial landforms such as cirques, glacial valleys, lakes on the plateaus, and the fjord basins with marked thresholds were formed. Today these features dominate the scenery in the western parts of the areas.

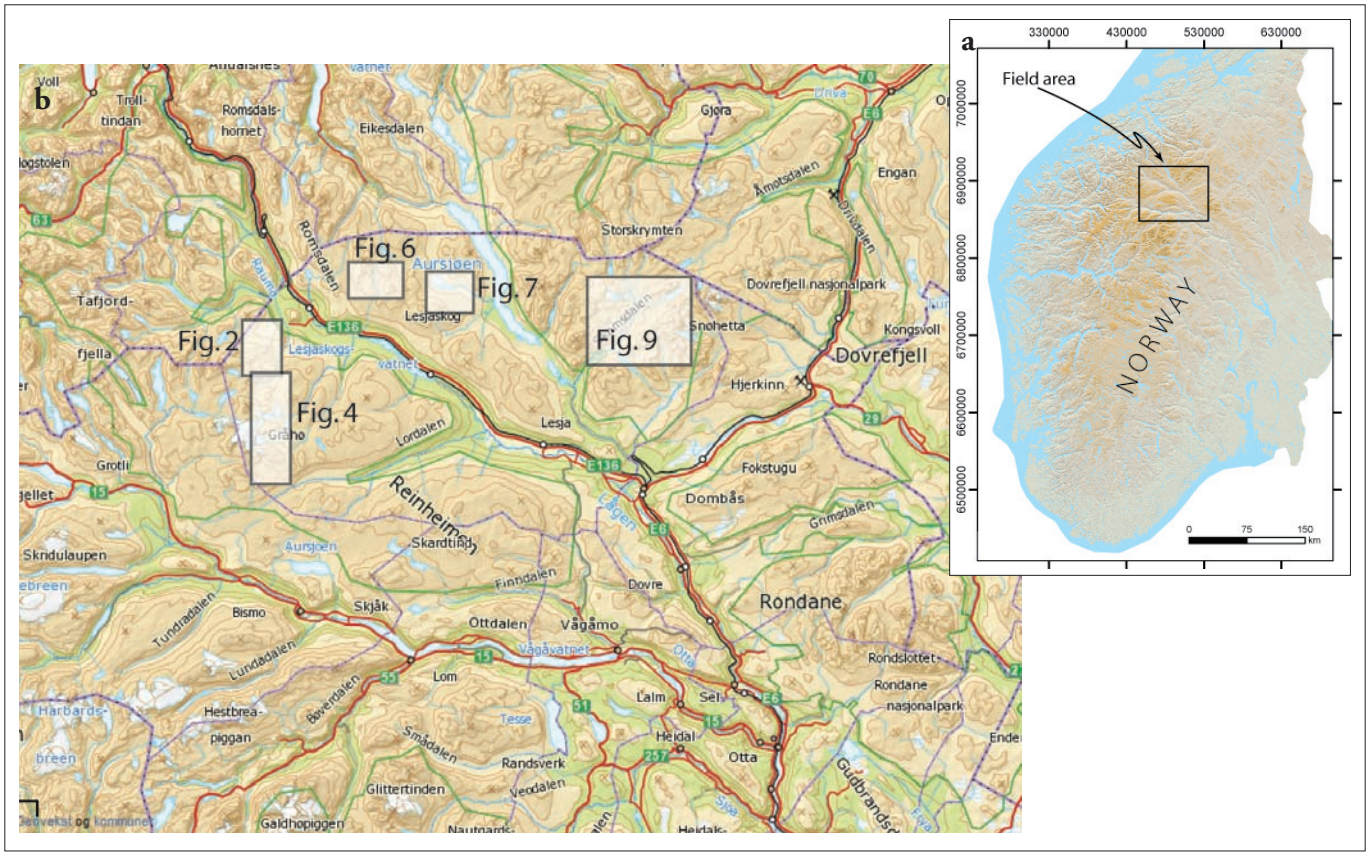

Figure 1. (a) Field area in central Norway. Coordinates are given in UTM 32N. (b) Orientation of key maps used in the description.

Reconstructing former ice extent based on ice marginal deposits

Ice marginal moraines (frontal and lateral moraines) are very diagnostic glacial landforms and directly reflect an ice marginal position (Benn and Evans 1998). In addition, since ice marginal moraines usually are formed and preserved during a glacial advance and retreat, they commonly reflect a significant climatic event. For example, global ice maximums and YD positions have been defined through mapping of ice marginal moraines (Mangerud 2004).

Undås (1963) made an attempt to establish the westward limit for the YD readvances in Western Norway based on the distribution pattern of terminal and lateral moraines. Since then, several authors have used glacial landforms such as lateral and end moraines for reconstructing the glacial chronology in Western Norway (e.g., Andersen 1954, 1960, Anundsen 1972, Follestad 1972, Vorren 1973, Fareth 1987). In the counties of Møre and Romsdal and Sør-Trøndelag similar reconstructions of the ice margin based on ice marginal deposits have been carried out by Sollid and Kristiansen (1984), Reite (1990, 1994), Follestad (1994), Follestad et al. (1994) and Mangerud et al. (in press).

Marginal moraines

Around the Romsdalen valley, well defined lateral moraines are shown in maps and are briefly described by Sollid and Kristiansen (1984).These marginal moraines in the communities of Lesja, Nesset and Sunndal further to the northeast and east, indicate a continuation of a more or less simultaneous glacier surface (Follestad 1987, 1994) in the areas of Gudbrandsdalen, Rondane and Skrymtheimen. Recent data compiled through the Geological Survey of Norway mapping program (Follestad 2006, 2008, 2010) suggest that we can divide these ice marginal deposits into upper and lower systems, which reflect two ice surfaces in the northwestern parts of Oppland County and the southeastern parts of Møre and Romsdal County, respectively. In the following some key localities will be described (Figure 1b).

Ice marginal deposits supporting an upper marginal zone in the eastern parts of the Romsdalen/Gudbrandsdalen valley

Grønhøi–Skarvehøi mountain (Figure 2)

In the area of the Grønhøi mountain (1462 m a.s.l.) a marked ice marginal zone is seen. The zone consists of several distinct lateral moraines, of which the distal moraine ridge reaches some 1380 m a.s.l. From this altitude the distal moraine ridge falls southwestward along the western side of the mountain into the valley west of the Rånåfly area. Here, the ice marginal zone is correlated with four distinct end moraines that run across the

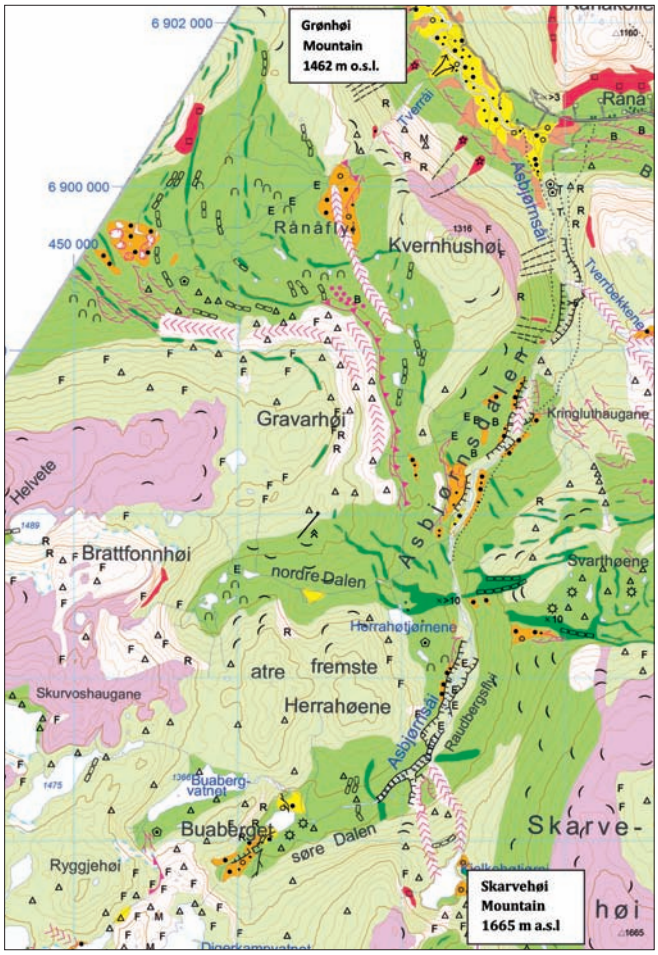

Figure 2. Lateral moraines shown in dark green are seen from the Grønhøi mountain (1462 m a.s.l.) in the northwest to the Skarvehøi mountain (1665 m a.s.l.) in the southeast. The figure is copied from the Lesja Community Map, M 1:80,000 (Follestad 2010). For use of colour and signs, see the map legend for Quaternary maps (Follestad 2010).

valley floor. The valley floor is situated at about 1200 m a.s.l.

As the horizontal distance for the distal moraines from the valley bottom to the top of the Grønhøi mountain is 1.3 km, this implies a surface gradient for the lateral moraine of about 150 m km^{-1}.

To the southeast the moraine zone continues along the northern flank of Gravarhøi mountain (1473 m a.s.l.). The distal moraine is 5–10 m high and consists of a diamicton with some blocks at the surface. Juxtaposed to the lateral moraine is a system of glacial meltwater channels (Figure 2). Since the meltwater channels exhibit the same gradient as the lateral moraine, we suggest that they were formed synchronously. These channels point towards the northwest and it seems probable that they represent the continuation of a large glacial drainage system, which has washed the rock surfaces along the northern and western slope of the Gravarhøi mountain a few metres below the uppermost distal lateral moraine. Further southeastward and into the Nordre-Dalen valley a set of lateral moraines shows the continuation of the same moraine zone. The distal moraine reaches an altitude of 1400 m a.s.l. on the eastern flank of Gravarhøi mountain, and falls thereafter into the valley of Asbjørnsdalen. The valley floor in the Asbjørnsdalen valley is situated at about 1200 m a.s.l. Since the horizontal distance for the distal moraines from the valley bottom to the top along the hillside of Gravarhøi mountain is 1.7 km, this gives a surface gradient for the distal lateral moraines of 130 m km^{-1}. In addition, from the Asbjørnsdalen valley to the Rånåfly area a marked erosion terrace, 5–20 m wide, was formed sub-/semi-laterally to the inland ice along the Gravarhøi mountain (Figure 3). This terrace shows that meltwater most probably followed the present course of the Asbjørnsåi river to the north, then turned northward and drained through the Rånåfly area during the deglaciation. Some 20 m below the erosion terrace, a marked area of washed bedrock is seen in the runoff pass between the Asbjørnsdalen valley and Rånåfly area. This feature, which can be followed northward for 1 km, cuts through the proximal lateral moraine. Thus the northward-draining meltwater channels from the Asbjørnsdalen valley show that a glacier surface higher than the hydrographic threshold existed in this valley, at the same time as when the ice already had disappeared in the westen parts of the Rånåfly area. Later, the glaciofluvial meltwater drainage turned eastward through the Asbjørnsdalen valley and ended in the distinct glaciofluvial deposit in the Asbjørnsdalen valley.

Furthermore in the Asbjørnsdalen valley, three 10–30 m-high lateral moraines (Figure 4) indicate the continuation of the ice margin to the east and south along the Skarvehøi mountain, which reaches altitudes of 1579 m a.s.l. and 1665 m a.s.l. in the northern and southern parts, respectively. The two well defined moraine ridges further south in the Søre-Dalen valley (the continuation of the Asbjørnsdalen valley to the southwest), are considered to have formed prior to the formation of the ice marginal zone.

A well developed ice marginal terrace situated 1300 m a.s.l. was formed between the distal lateral moraine and the northern mountain side of Skarvehøi from meltwater which followed the meltwater channel distally of the moraine ridge. An obvious glaciofluvial deposit is situated at the same altitude in Søre-Dalen valley (the upper parts of the Asbjørnsdalen valley), which indicates that a ice-dammed lake was formed here during the formation of the moraine zone.

Skarvehøi mountain–Løyfthøene mountain

A well defined ice marginal zone consisting of lateral moraines is seen in the areas north and east of the Skarvehøi mountain (Figure 5). The distal lateral moraine is 3–10 m high and consists of coarse diamicton with blocks at the surface. This moraine can be followed continuously from 1400 m a.s.l. in the north to 1540 m a.s.l. south of Skarvehøbotn (1462 m a.s.l.).

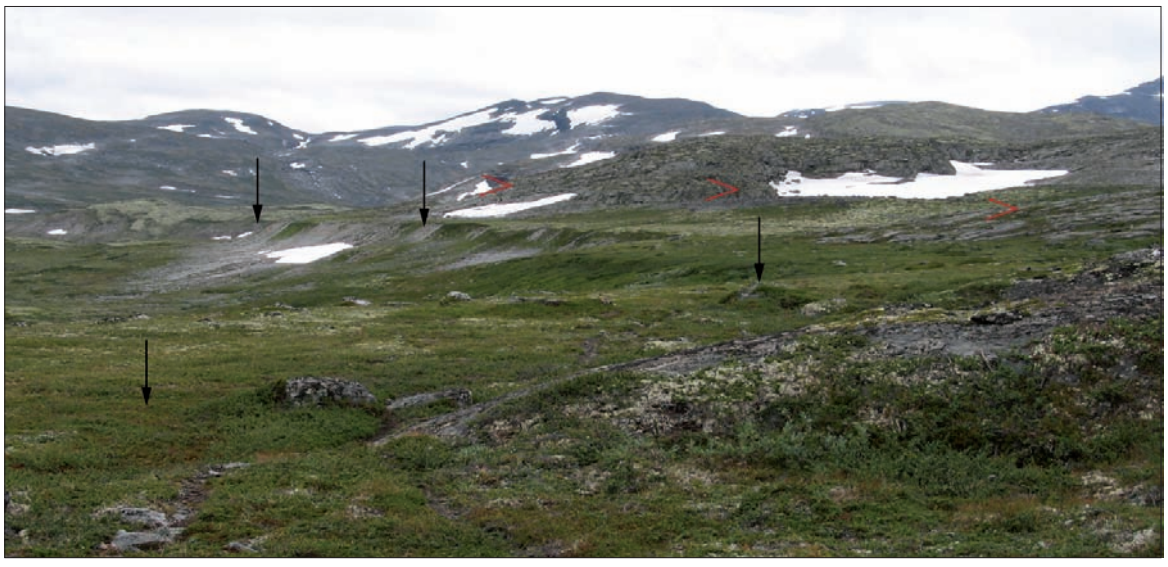

Figure 3. A marked erosion terrace is seen along the lower part of the Gravarhøi mountain. The front of the terrace is indicated by the black arrows. The proximal rock surface is washed and eroded by meltwater. The altitude of the terrace is determined by the rock threshold in the front of the photo. The photo is taken from the threshold in the northern part, looking southward.

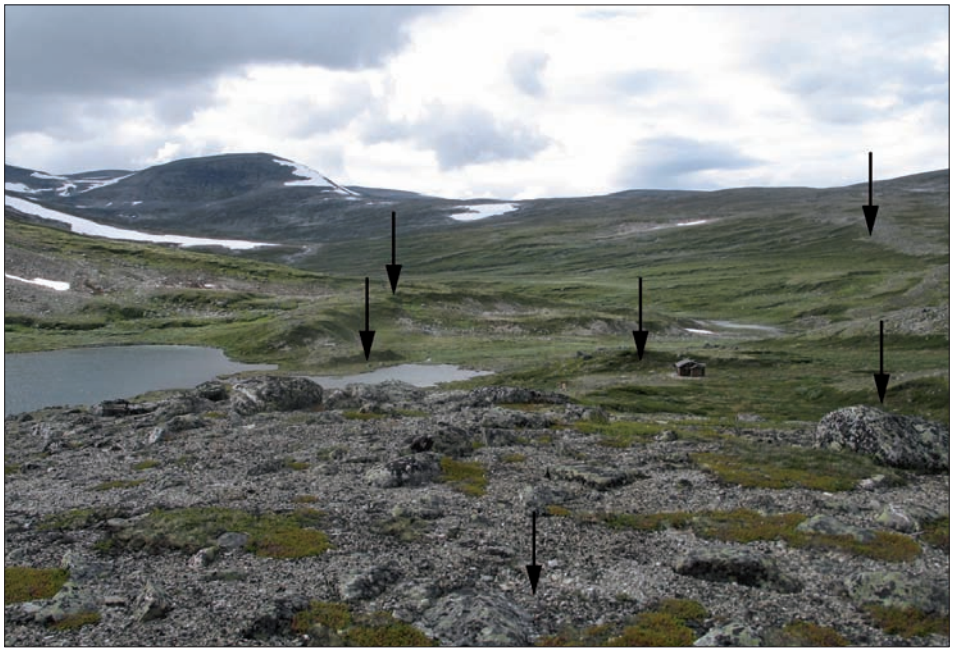

Figure 4. Marked lateral moraines at the ice marginal zone east of Herrahøtjørnene lakes. The ridges are up to 30 m high. The photo is taken from the lateral moraine east of Herrahøtjørnene, looking west.

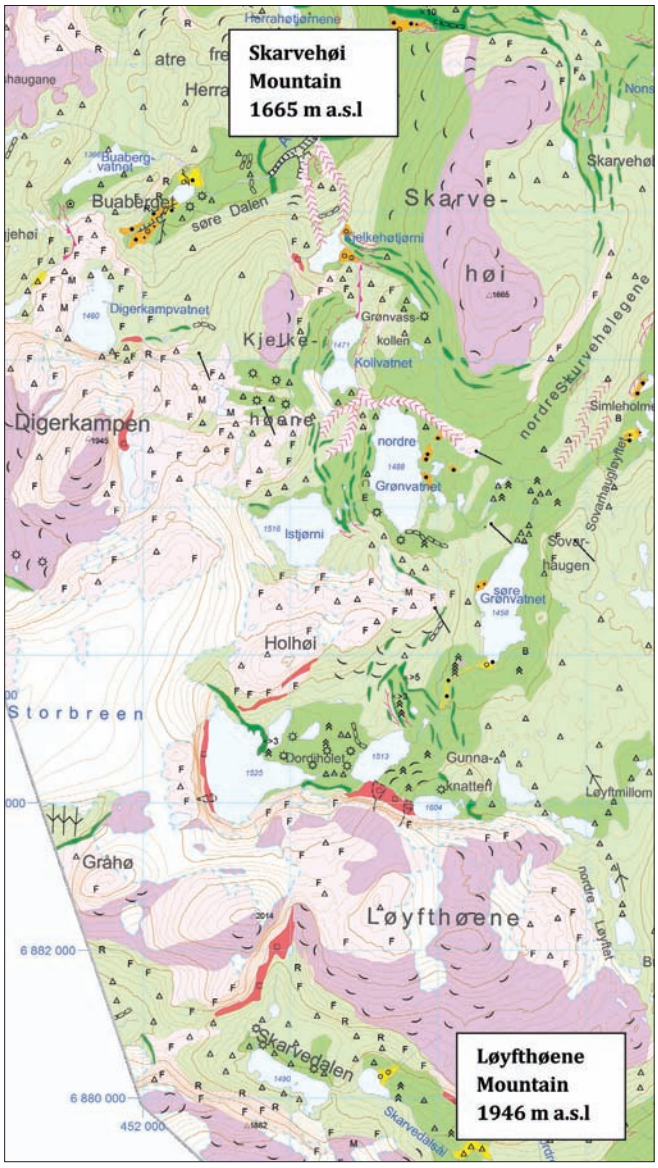

Figure 5. Lateral moraines shown in dark green as seen from the Skarvehøi mountain (1665 m a.s.l.) in the north to the Løyfthøene mountain (1579 m a.s.l.) in the south. The figure is copied from the Lesja Community Map, M 1:80,000 (Follestad 2010). The grid net is based on the M711 map series with a grid cell size of 1 km x 1 km. For use of colour and signs, see the map legend for Quaternary maps (Follestad 2010).

Since the horizontal distance is 5 km and the altitude difference is 140 m, this gives a slope gradient of 28 m km^{-1} for the distal moraine. The meltwater channels northeast of Skarvehøi mountain formed simultaneously with the moraine zone, but somewhat later than the distal moraine. It should also be noted that the moraine zone here is formed only a few metres below the allochthonous block fields seen in the Skarvehøi areas and marked with violet colour in the Quaternary maps.

To the southwest of Skarvehøi mountain the continuation of the glacier margin is again shown by a continuous moraine zone. This consists of 2–3 marked lateral moraines which fall into the areas of the Kolvatnet lake and the Kjelkehøtjønne lake (1397 m a.s.l.). The altitude of the distal moraines is at 1580 m a.s.l. at the southern valley side of Skarvehøi mountain and 1400 m a.s.l. in the area of Kjelkehøtjønne lake. In all this implies a slope gradient of 72 m km^{-1}.

At the northern side of Kjelkehøtjønne lake, there are two areas with significant glaciofluvial washing and scouring. These features can be followed continuously to the base of Søre-Dalen valley to the north. This indicates that water runoff continued in this direction for some times after the breakup of the suggested ice-dammed lake.

From the Kjelkehøtjønne lake (1397 m a.s.l.) a distinct lateral moraine follows the eastern side of the Kjelkehøi mountain (1692 m a.s.l.) and points at a continuation of the ice margin into the Istjørni lake (1514 m a.s.l.) areas. Since

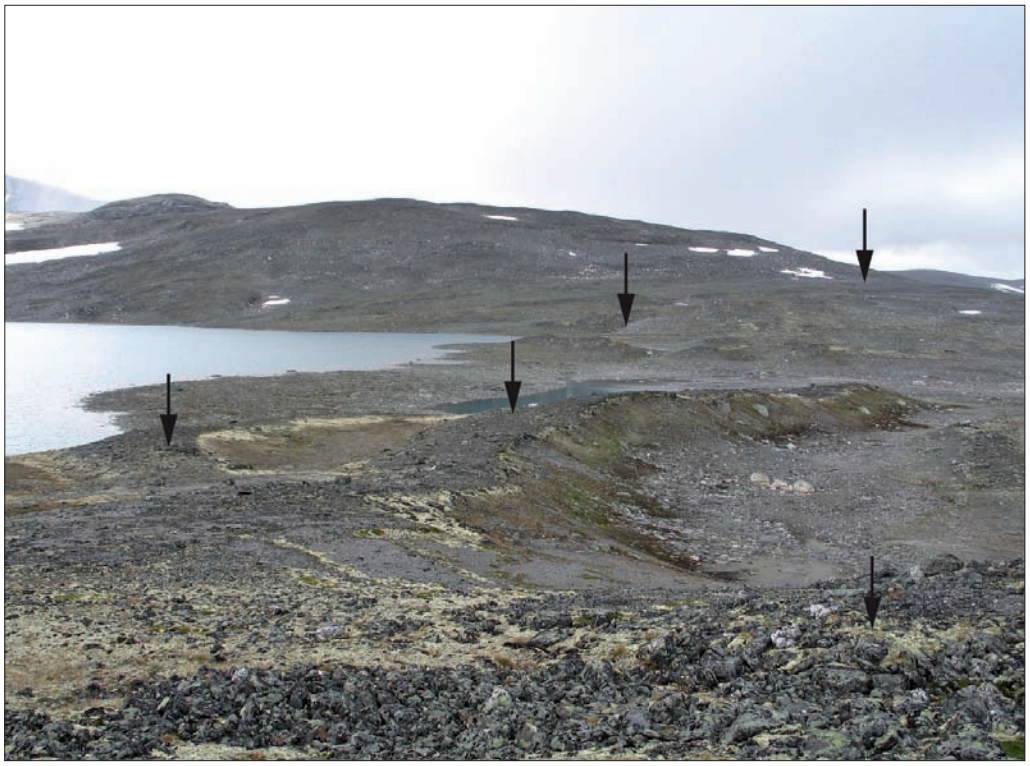

Figure 6. Marked lateral moraines are seen in the rand zone east of the Istjørni lake. The ridges can here be up to 20 m high. The photo is taken from the lateral moraine east of Istjørni lake, looking northwest.

the distal moraine reaches an altitude of 1580 m a.s.l. and the vertical altitude is 66 m over a horizontal distance of 1 km, this gives a surface gradient of 66 m km^{-1}. In the Istjørni lake area the distal moraine is very distinct and 5–10 m high (Figure 6).

Further on, from the Istjørni lake area, an obvious lateral moraine can be followed along the eastern flank of the Holhøe mountain (1806 m a.s.l.). At this site, the distal lateral moraine reaches an altitude of 1580 m a.s.l. before falling southward

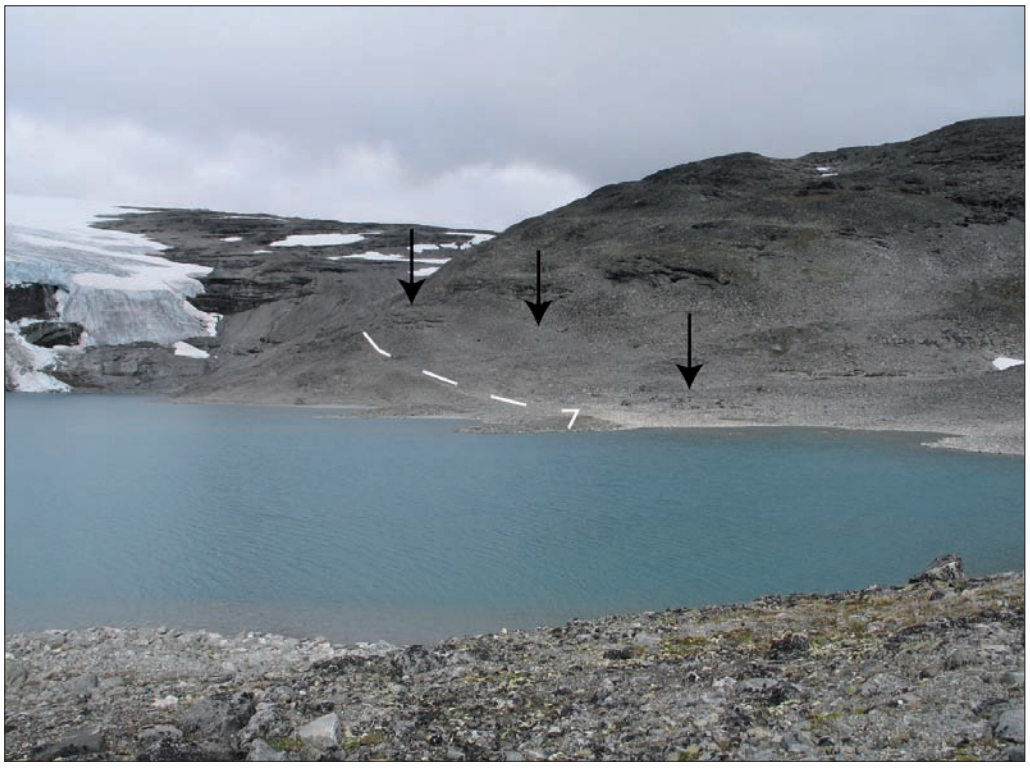

Figure 7. Two lateral moraines are seen in the front of the glacier outlet in the Dordihol area, here marked with arrows and a white dashed line. Photo is taken from the distal moraine, looking westward.

into the area east of "unnamed lake" (1513 m a.s.l.) in the Dordiholet area. The vertical distance between these localities is 67 m and the horizontal distance some 1.5 km, which gives a slope gradient of 42 m km^{-1} for the distal lateral moraine ridge. Further to the south a lateral moraine can be followed along the northern side of Løyfthøiene mountain (1921 m a.s.l.) up to an altitude of 1610 m a.s.l. Here, further evidence for a moraine zone is missing. However, the marginal moraines shown in the areas southwest of Storbreen glacier and in the Storvatn lake (1495 m a.s.l.) might represent a continuation of the marginal system in a westward direction (Sollid and Kristiansen 1984).

Also in the areas of Istjørni and Dordiholet lakes, fresh-looking lateral moraines are observed. Around the Dordiholet lake (Figure 7) two terminal moraines are seen, which indicates that the Storbreen glacier has reached further east than the present extent. However, since there are no signs that outlet glaciers from the area occupied by the present Storbreen glacier reached into the described moraine zone, these 'fresh-looking' lateral moraines are considered to be young and representative for the Little Ice Age readvance around AD 1750 or later.

Summary and conclusions

From the above descriptions we document an ice marginal zone consisting of well defined lateral moraines in the alpine areas of Grønhøi–Skarvehøi–Løyfthøene along the southern valley side of Romsdalen and Gudbrandsdalen valleys. Furthermore, it is documented that the glacier branches shown by the distal lateral moraines in the valley west of Rånåfly, in the valley of Nordre-Dalen and in areas east of Kjelkehøene mountain and in the basin of the Istjørni lake, have steep slope gradients (with a range from 150 m km^{-1} to 40 m km^{-1}) which are characteristic of advancing glaciers. Within the ice marginal zones, marked meltwater landforms are seen in the westerly areas. The distal lateral moraines in the areas of the Skarvehøi mountain reach an altitude of 1540 m a.s.l., which is only some tens of metres below the mountain areas dominated by allochthonous block fields. Since this type of superficial deposit is considered to have survived under cold-based glacier ice (e.g., Kleman and Hättestrand 1999, Stroeven et al. 2002), it is suggested that the transition from cold-based ice to warm-based ice was at about 1550 m a.s.l. Thus the temperature regime at that time is thought to have been closer to a sub-arctic climate than an arctic climate.

Ice marginal deposits supporting an upper marginal zone north of the Romsdalen/Gudbrandsdalen valley

The Svarthøi mountain–Storhøi mountain (Figure 8)

In the mountain areas northeast of the Romsdalen/Gudbrandsdalen valley an ice marginal zone consisting of distinct lateral moraines (Figure 8) can be found in the areas south of the Svarthøi mountain. The lateral moraines follow the southern flanks of the mountains nearly continuously from the

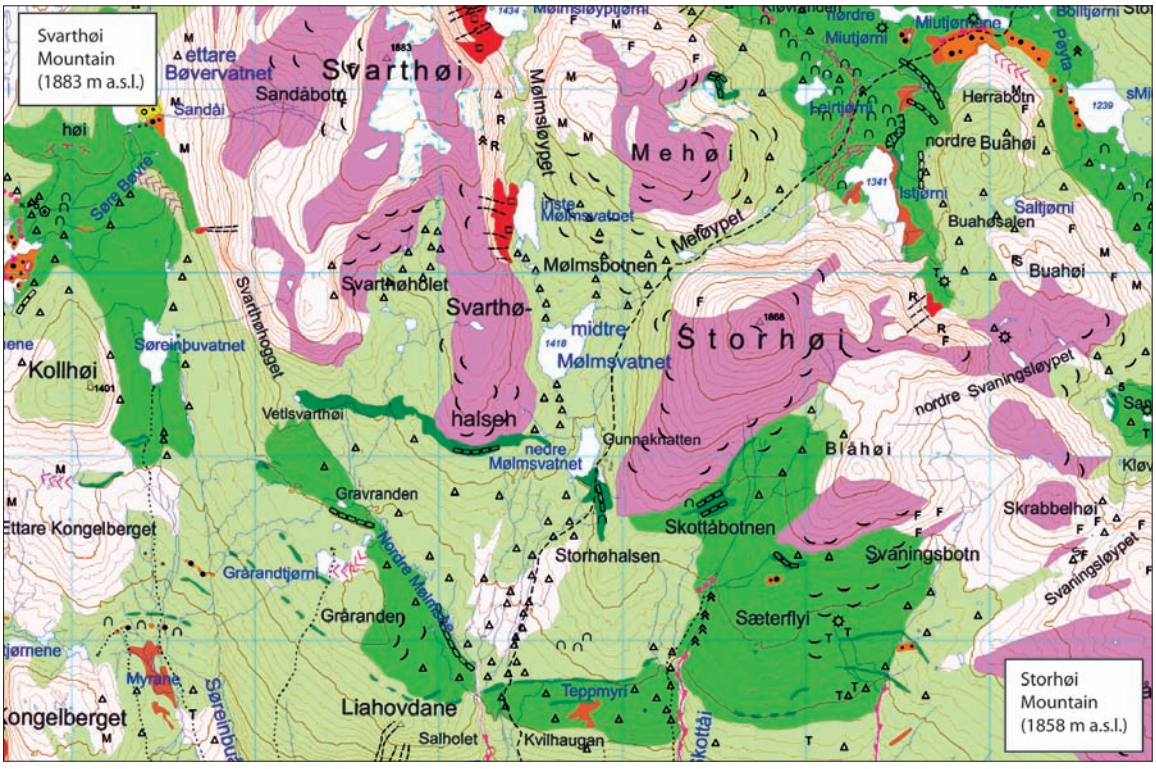

Figure 8. Lateral moraines shown in dark green as seen from the Svarthøi mountain (1883 m a.s.l.) in the northwest to the Storhøi mountain (1858 m a.s.l.) in the east. The figure is copied from the Lesja Community Map, M 1:80,000 (Follestad 2010). The grid net is based on the M711 map series with a grid cell size of 1 km x 1 km. For use of colour and signs, see the map legend for Quaternary maps (Follestad 2010).

Figure 9. Two distinct end moraines were formed in the western parts of the Sandåflatene area, here damming a small lake. The distal moraine is up to 15 m high (cf., the red rowboat, which is 3 m long). The proximal ridge seen in the lake is 3–5 m high. The forms of the moraines indicate that they were deposited along a glacier outlet entering the areas from the west. Photo is taken from the distal moraine towards south.

Svarthøi mountain to the Svarthøhalsen mountain and further to the east. The distal moraine is 2–4 m high and consists of gravelly to sandy till with blocks and boulders at the surface. Distally to the moraine ridges some minor lateral meltwater channels can be seen. The most prominent features are seen in the areas south and west of the Bøvervatnet lake where washed rock surfaces together with some glaciofluvial deposits indicate a westward run-off direction. However, the number of lateral meltwater channels is low compared to the number of meltwater channels seen in the areas of Asbjørnsdalen valley (Figure 2).

In the areas south of Svarthøi mountain the distal moraine is situated at 1420 m a.s.l. In an eastward direction the altitude

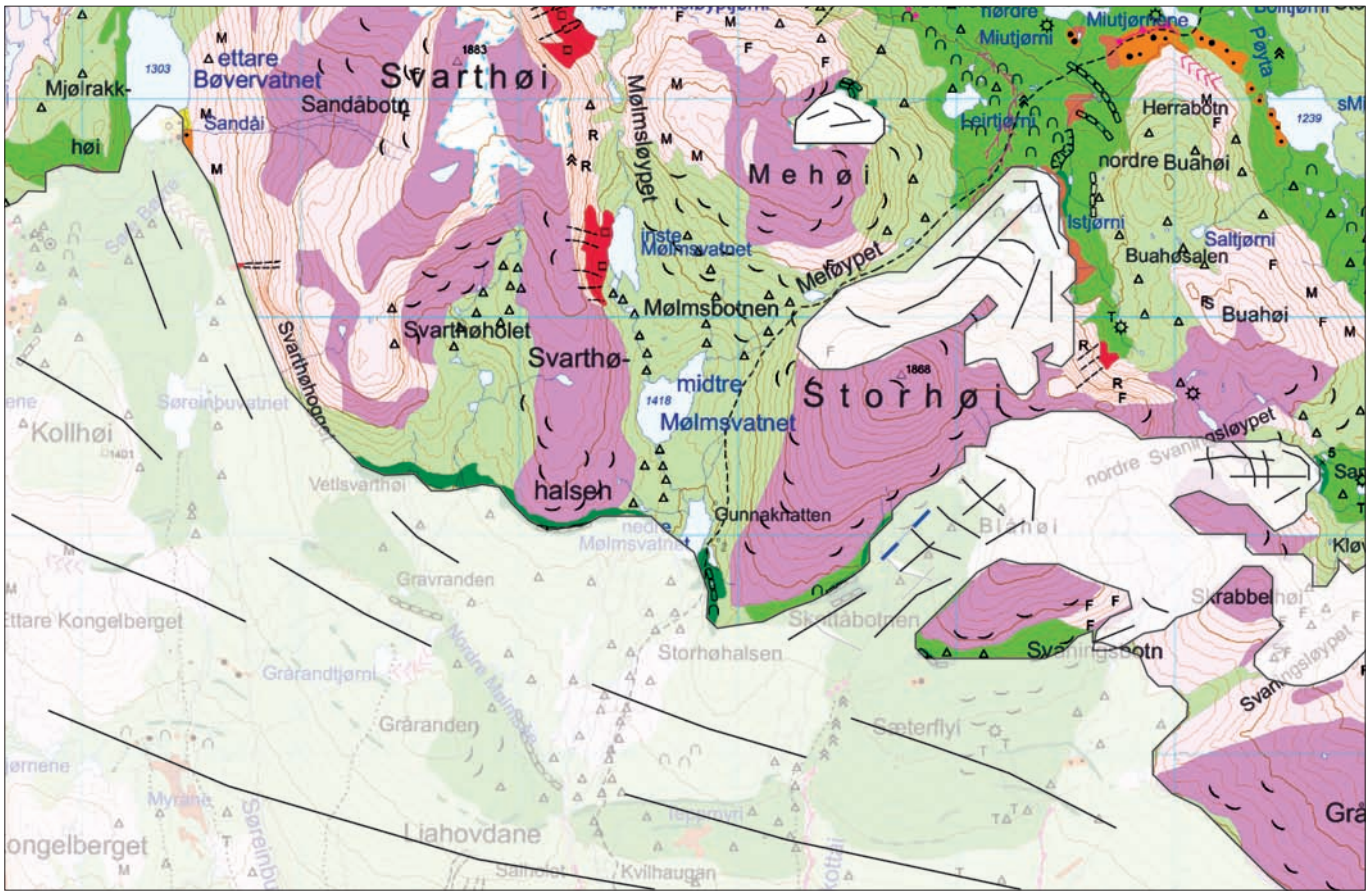

Figure 10. A tentative reconstruction of the suggested plateau glacier in the areas of the Storhøi mountain. Outlet glaciers are indicated to the southwest (against the Romsdalen/Gudbrandsdalen valley) and to the east against the Sandåflatene area from the plateau of the Storhøi mountain. For use of colour and signs, see the map legend for Quaternary maps (Follestad 2010).

of the distal moraine rises to about 1460 m a.s.l. at the Svarthøhalsen mountain. Southeast of the Storhøi mountain (1868 m a.s.l.) distal lateral moraines reach an altitude of 1480 m a.s.l. Since the distance from the areas south of Svarthøi mountain to the Storhøi mountain is 4.5 km and the difference in altitude is 60 m, this gives a slope gradient for the distal moraine of 13 m km^{-1}.

From the marginal zone southeast of Storhøi (Figure 8), a lateral moraine can be followed northwards into the valley between the mountains of Storhøi and Blåhøe (1668 m a.s.l.). This lateral moraine terminates at an altitude of 1560 m a.s.l. The gradient for this lateral moraine is calculated to about 80 m km^{-1}.

North and east of the Storhøi mountain plateau, distinct end moraines are seen in the Istjørni lake (1341 m a.s.l.) and the little lake west of Sandåflatene, east of the plateau of the Storhøi mountain (Figure 9). Cirque glaciation simultaneous with the formation of the lateral moraines along the Romsdalen/Gudbrandsdalen valley might explain the formation of the end moraine in the Istjørni lake. However, no sign of a cirque glaciation is seen in the areas west of the Sandåflatene area. Instead, we argue that the most reasonable explanation for these moraines is formation from an outlet glacier emanating from the plateau and terminating in the lake, as indicated in the tentative reconstruction of the ice margin (Figure 10).

The Vangshøi mountain–Vangsvatnet lake–Aursjøen lake

In the areas of the Vangsvatnet lake (Figure 11) a very well defined ice marginal zone can be observed. The distal lateral moraine is very pronounced (Figure 12). It can be followed nearly continuously from 1310 m a.s.l. on the northeastern slope of the Vangshøi mountain to northern end of the Vangsvatn lake (1166 m a.s.l.), over a distance of more than two kilometres. The upper boundary for a continuous cover of till might indicate a possible continuation of the lateral moraine to the southeast for another 0.5 km. The corresponding ice margin on the mountain slope southeast of Vangshøi mountain would be at an altitude of about 1530 m a.s.l., assuming a slope gradient of 13 m km^{-1}. The horizontal distance from the lateral moraines in the Storhøi area is about 4 km. This indicates that the lateral moraine seen at 1380 m a.s.l. is too low to justify a simultaneous formation to the uppermost ice marginal zone. Thus the deposit is assigned to the formation of the lower ice marginal zone seen in the areas of the Romsdalen/Gudbrandsdalen valley.

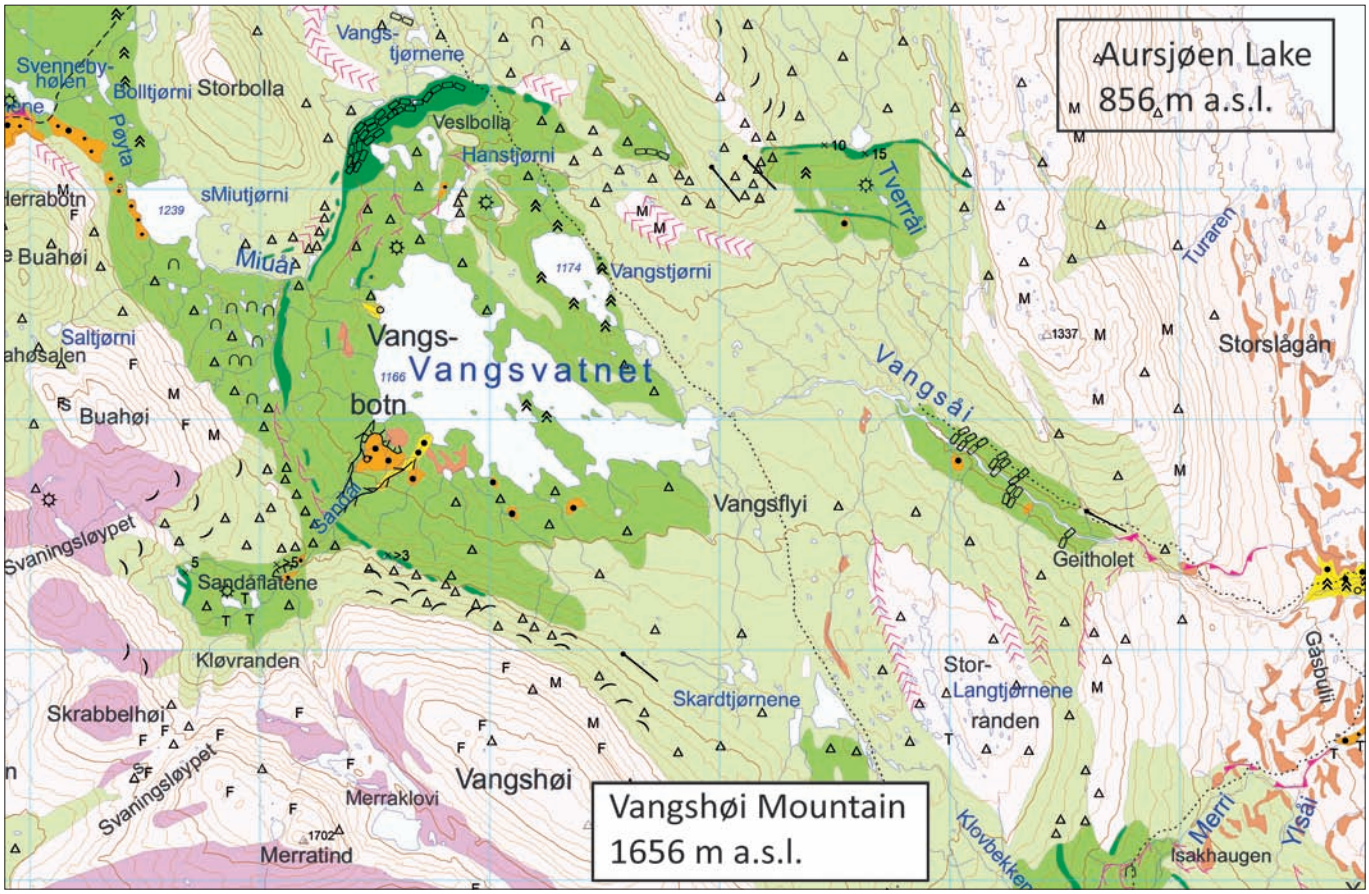

Figure 11. The ice marginal zone in the Vangsvatnet lake areas. For use of colour and signs, see the map legend for Quaternary maps (Follestad 2010).

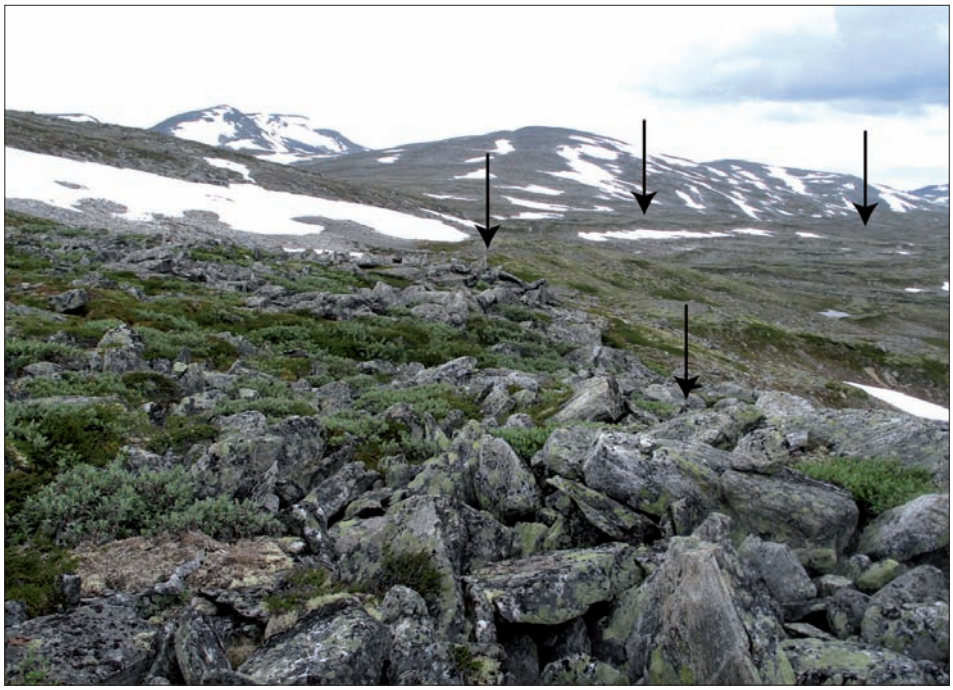

Figure 12. The lateral moraine along the northeastern hillside of Vangshøi mountain. The moraine ridges are characterised by a sandy gravely matrix with blocks on the surface. In some cases the sandy gravely matrix is washed away, leaving the blocks as a lag deposit. The Vangsvatnet lake is seen to the right. The photo is taken from the distal moraine, looking eastward.

To the north, in the valley of Vangsvatnet lake, a marked end moraine occurs. This end moraine consists of several distinct moraine ridges. Some of the ridges consist of a sandy matrix with blocks on the surface, while other ridges are blocky throughout (Figure 13). Commonly glacial meltwater channels run between the moraine ridges. This in turn indicates that meltwater was present during the formation of the lateral moraines.

In the Miua valley, west of the Vangsvatnet lake, there is a marked area of continuous till cover with blocks and mounds continuing northwestward into the Pøyta area. Here some marked glaciofluvial lateral terraces have been formed when the meltwater drained through this valley to the north. These forms, together with the end moraines west of Sandåflatene (Figure 10), show that the glacier tongue in the Vangsvatnet area never penetrated into these areas during the formation of the lateral moraines. Thus the ice margin north of the Vangsvatnet lake is most likely simultaneous with the described ice marginal zone in the Romsdalen/Gudbrandsdalen valley.

Figure 13. Lateral moraines northwest of the Vangsvatnet lake.

From the ice marginal position north of the Vangsvatnet lake two distinct lateral moraines in the Tverråi areas show the further continuation of the ice marginal zone into the Aursjøen area. These lateral moraines are commonly more than 10 m high and consist of a gravelly sand matrix with blocks at the surface. The uppermost lateral moraine ends in the steep valley side of Aursjøen (856 m a.s.l.) at an altitude of 1320 m a.s.l. As the distance between the end moraines in the Vangsvatnet area to the lateral moraines along the southern side of the Aursjøhøi mountain is 2 km, this gives a gradient of some 75 m km^{-1}.

On the steep valley side of the Aursjøen lake (856 m a.s.l.) no marginal deposits have been observed south of the Nesset area (cf., Follestad 1994).

However, indications of a possibly simultaneous inland ice are seen in the tributary valleys along the eastern side of the Aursjøen lake. In the Geitådalen valley, a marked lateral moraine occurs east of Grynningskampen (1549 m a.s.l.) at an altitude of 1520 m a.s.l. The lateral moraine can be followed continuously for one kilometre, to an altitude of 1500 m a.s.l. (20 m km^{-1}). A gradient of this magnitude leaves us with an ice surface that indicates that the end moraines west of lake 1423 m a.s.l. might have formed simultaneously. On the southern flank of the Geitådalen valley two marked end moraines can be seen some at 1410 m a.s.l., in front of a marked cirque valley. As this altitude is about 100 m below the extrapolated ice surface, they are considered to be younger than the above described moraines. Southwest of the Aursjøen lake marked lateral moraines at lower altitudes are seen at the mouth of Vangsvatn valley (Figure 11) and in the valley of Veslsvartådalen. These moraines might be synchronous with the lower ice marginal zone in the Romsdalen/Gudbrandsdalen valley (see below).

The lower ice marginal zone in the Romsdalen/Gudbrandsdalen areas

A lower ice marginal zone is seen along the northern, south-facing valley side of Romsdalen/Gudbrandsdalen valley. In the following a brief description is given, starting with the deposits south of the Romsdalen/Gudbrandsdalen valley.

The Asbjørnsdalen–Grøndalen valley

In these areas a pattern of marked lateral moraines trending west-, north- and eastward of the Nonshøi mountains seem to represent deglaciation ice margins (Figure 14). The ice marginal zone is situated approximately 200 m below the upper marked zone along the northern flank of the Skarvehøi mountain (Figure 2). The different ridges in the zone can be followed continuously for some hundreds of metres and are several metres high. They consist of a gravely sandy matrix, with blocks on the surface.In the Grøndalen valley the glacier in the main Romsdalen/Gudbrandsdalen valley dammed the rivers in the Grøndalen valley and glaciofluvial deposits were formed in sub-/semi-lateral positions. These deposits are seen at an altitude of 1200–1160 m a.s.l. and 1100–1080 m a.s.l., respectively. In connection with the lowest glaciofluvial deposits, several marked meltwater channels are seen (Figures 14 and 15).

The morphology and the westward run-off direction of the meltwater channels show that they are eroded in a sub-/semi-lateral position to an ice surface in the Romsdalen/Gudbrandsdalen valley falling in this direction. As the meltwater channels were formed nearly parallel to the lateral moraines, even though a few of the channels cut through some of the lateral moraines, they are considered to have a nearly simultaneous origin.

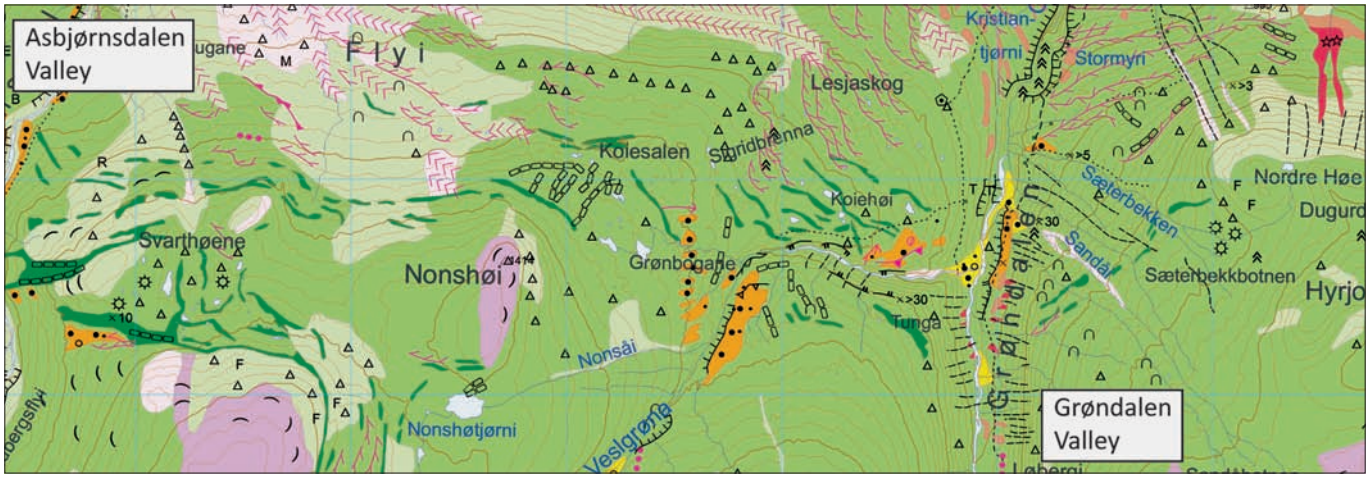

Figure 14. Lateral moraines shown in dark green as seen from the Asbjørnsdalen valley to the Grøndalen valley in the east. The figure is copied from the Lesja Community Map, M 1:80,000 (Follestad 2010). For use of colour and signs, see the map legend for Quaternary maps (Follestad 2010).

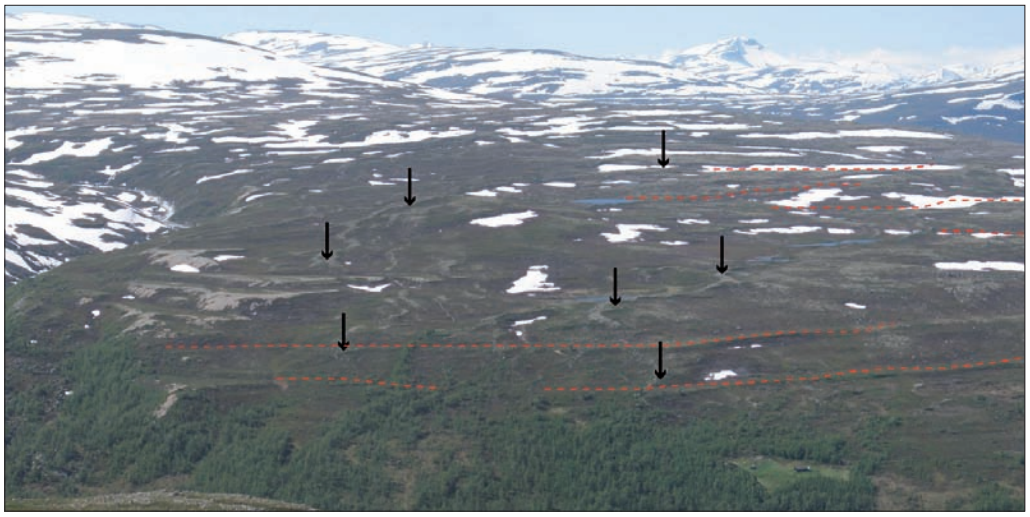

Figure 15. Laterally formed moraine ridges representing the lower rand zone in Romsdalen/Gudbrandsdalen valley are seen west of the Grøndalen valley (marked with black arrows). Several lateral meltwater channels were formed in these areas during and after the formation of the lower rand zone (red dots). Glaciofluvial terraces were formed marginal (or sub-/semi-lateral) to the ice margin when the inland ice was shrinking. The lowest terrace are seen to the left. Photo is taken from the eastern valley side of Grøndalen, looking westward.

A marked bending and change of run-off direction for the meltwater channels are seen at 800 m a.s.l. along the eastern side of the present river Grøna. This shows that behaviour of the meltwater changed when ice in the main valley had melted down to a thickness of about 200 m. The same changes in run-off direction are also seen in the areas east of the Asbjørnsdalen valley. Further eastwards, no obvious lateral moraines have been observed. However, the marked glaciofluvial deposit formed in the south of the Kampen mountain (1369 m a.s.l.) at an altitude of some 1320 m a.s.l., might indicate a continuation of the lower ice marginal zone.

In the Lordalen valley marked lateral moraines are seen along the northern and southern valley sides. Along the northern slope a lateral moraine more than 3–5 m high can be followed 1 km to the east along the southeastern side of Digervarden (1778 m a.s.l.). This lateral moraine is situated at approximately 1400 m a.s.l. in the central parts. The morphology and position in the terrain of the moraine ridge point at a likely formation by a valley glacier coming through the Lordalen valley. Along the southern side of the Lordalen valley, several distinct lateral moraines form a well defined ice marginal zone in the outermost parts of the Lordalen valley. The most marked distal lateral moraine is 2–4 m high and is situated at 1420 m a.s.l., northeast of Sletthøi mountain (1536 m a.s.l.). Further to the east two minor ridges are seen, reaching some 1560 m a.s.l.

Liahovdane

Marked lateral moraines are seen along the valley sides west and east of Liahovdane (Figure 8) from the Grårandtjønne lake (1281 m a.s.l.) to the Gråhøi mountain (1565 m a.s.l.) in the east. In these areas the lateral moraines reach an altitude of 1280 m a.s.l. and 1380 m a.s.l., respectively. Since the distance between the Grårandtjønne lake and the deposits at Gråhøi mountain is 7 km, the slope gradient is 14 m km^{-1} for the lower-lying marginal zone.

In the northeastern end of the Merrabotn valley lateral moraines have been deposited by glaciers flowing in the valleys of Merrabotn, Ylsbotn and Aursjøen. These moraines are situated at 1225 m a.s.l., east of the mountain peak 1258 m a.s.l. The moraine ridge deposited through the Merrabotn valley can be followed about 500 m to the northwest, where it reaches an altitude of 1275 m a.s.l. on the northeastern side of the Måni mountain. To the north this moraine is cross-cut by a lateral moraine deposited by a glacier, which came into this area through the Aursjøen valley. This clearly demonstrates that the ice movement through the Aursjøen valley took place somewhat later than the movement through the Merrabotn valley. The northward continuation of this former glacier is given by the marked 3–5 m-high lateral moraines which cross the Merraboten valley. North of the Merri river, these lateral moraine ridges are 2–10 m high. Further northwards moraine ridges, seen in the valley of the Vangsåa river, might have been deposited more or less simultaneously with the lateral moraines in the Merrabotn areas.

Summarising discussion

The above descriptions from the valley flanks of the Raumadalen and Gudbrandsdalen valleys illustrate that an ice marginal zone some 200 m below the upper ice marginal zone seems to have been deposited during the deglaciation. Sets of meltwater channels were formed simultaneously and follow the lateral moraines closely down to about 800 m a.s.l. At that time the ice remnant in the main valley was only about 200 m thick.

Profiles with projected lateral moraines in the Romsdalen/Gudbrandsdalen areas

In the Raumadalen/Gudbrandsdalen areas the lateral moraines, as seen in Figure 16, are projected and plotted in digital elevation profiles (Figures 16 and 17). Lateral moraines occur along

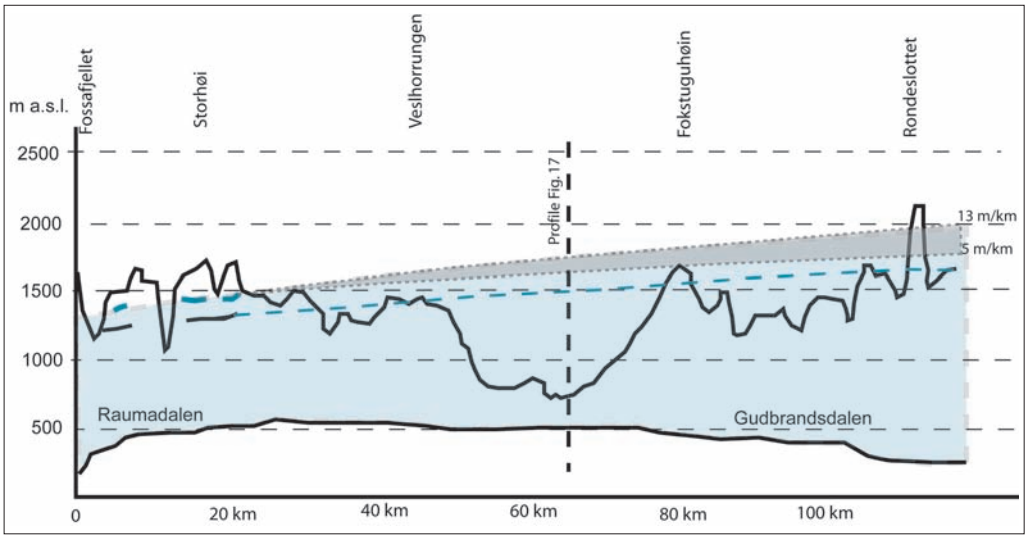

Figure 16. Reconstruction of a tentative glacier profile on the basis of lateral moraines which are projected and plotted in digital elevation profiles. The upper and lower ice marginal zones are shown and extrapolated in a southeastward direction.

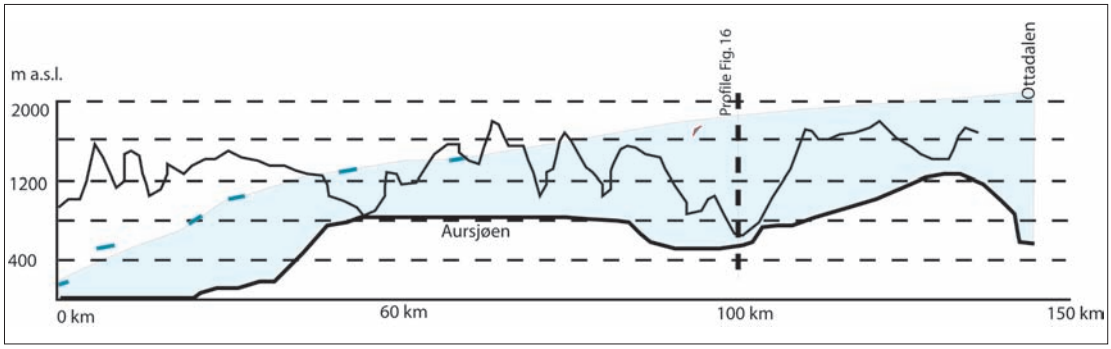

Figure 17. Reconstruction of a tentative glacier profile on the basis of lateral moraines which are projected and plotted in digital elevation profiles through the Eresfjord–Aursjøen lake valley to the valley of Gudbrandsdalen and further southwestward through the valley of Lordalen to the Otta valley. The upper ice marginal zones are shown and extrapolated in a southeastward and southwestward direction.

the mountain sides of the valley Raumadalen from the Hatten mountain area to the Skarvehøi mountain in the valley of Gudbrandsdalen (Figure 16). As the Hatten lateral moraines are situated at 1250 m a.s.l. and the moraines along the Skarvehøi mountain are some 1580 m a.s.l. (over a distance of 21 km), this gives a slope gradient of 15 m km^{-1} for the valley glacier. The glacier thickness is about 1000 m to the west and 1200 m at the mouth of Lordalen valley.

If a similar tentative glacier profile is constructed on the basis of lateral moraines in the areas of the Aursjøen lake to the Gudbrandsdalen valley and southward through Lordalen valley to the valley of Otta (Figure 17), a marked drop in the lateral moraines is here seen west of Aursjøen lake (to the left in Figure 17). In the Aursjøen lake areas the lateral moraines indicate an ice surface some 1300 m a.s.l. and a thickness of the glacier of some 500 m. In the Gudbrandsdalen areas and southward through the Lordalen valley, the surface of the ice continues to rise (if we use a gradient of 28 m km^{-1}). In the areas of the Ottadalen valley the surface of an inland ice would be more than 2000 m.

The marginal zones in the areas east of lake Aursjøen

The scenery of these areas is dominated by mountains, reaching up to 2000 m a.s.l. (Figure 18). The valley of the Jori river and its tributary valleys run through the area. In the sides of the valleys lateral moraines were formed. These moraines show that a glacier outlet from the inland ice penetrated the area. Distinct lateral moraines are seen along the mountain of Skulan (1690 m a.s.l.) and Salhøe (1767 m a.s.l.). The lateral moraines are here situated 1460 m a.s.l. in the west and 1420 m a.s.l. in the eastern areas. As the distance between the measured points are 2.5 km this leaves us with a gradient of 16 m km^{-1} for the glacier falling into the upper parts of the Åmotdalen valley. The valley floor is here at some 1361 m a.s.l. in the area of lake Drugshøtjønnin. Together with the altitude of the lateral moraines (1420 m a.s.l.) this shows that the valley glacier was 60 m thick when these lateral moraines were deposited.

In the areas of Nedre Lustjørni lake there are several well defined moraine ridges. These ridges, which are 2–10 m high, have ice contact faces to the west indicating that a glacier flowed

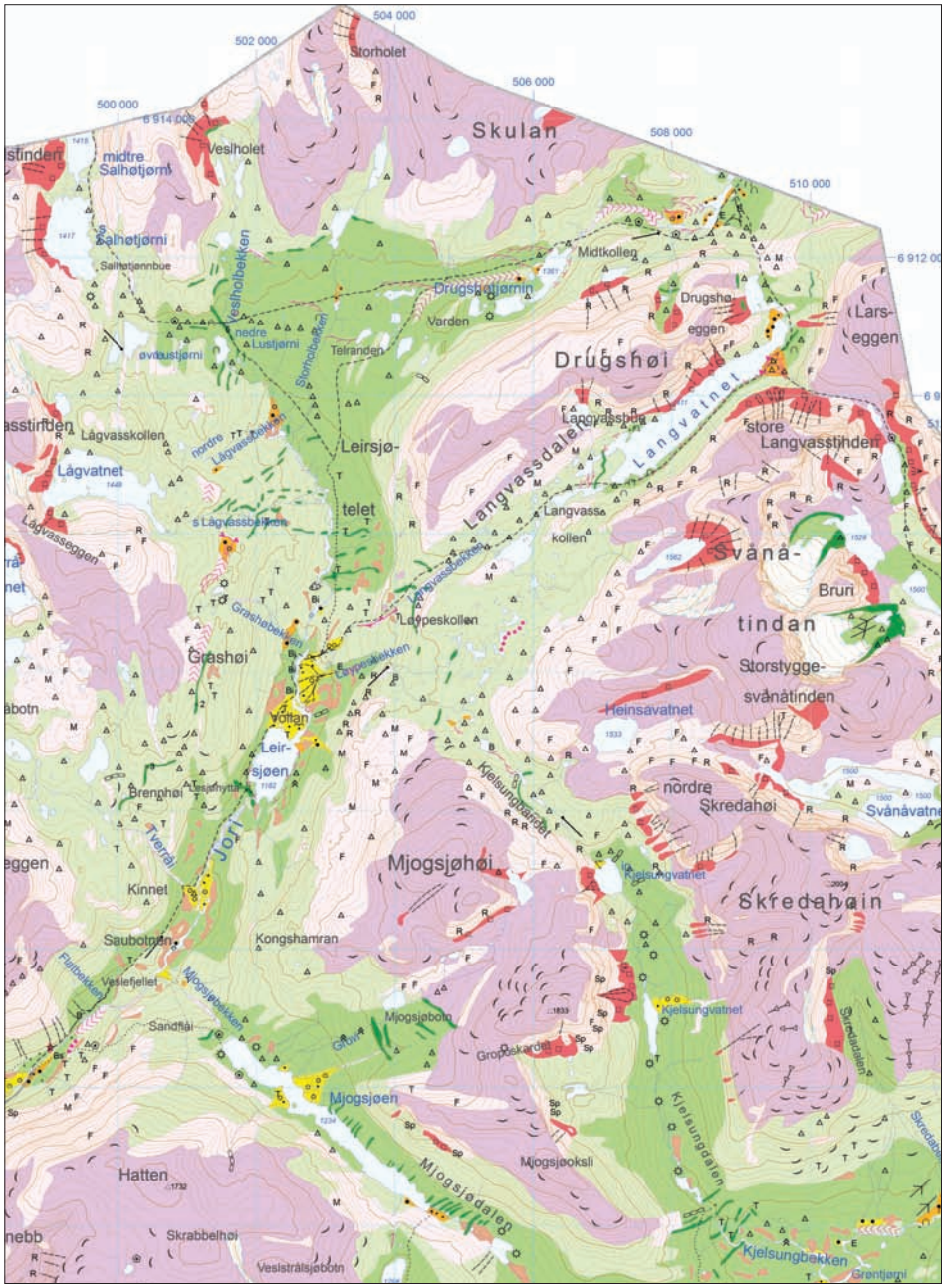

Figure 18. Lateral moraines shown in dark green are seen in the upper parts of the Jori river valley (Skamsdalen valley/Langvatnet lake valley). In the mountains of Svånåtindan the terrain reaches an altitude of 2000 m. The map is copied from the Lesja Community Map, M 1:80,000 (Follestad 2010). For use of colour and signs, see the map legend for Quaternary maps (Follestad 2010).

into the upper parts of the Jori river valley from the west. The formation of these moraine ridges took place somewhat later than the formation of the lateral moraines along the valley side of the mountains Skulan and Salhøe.

West of the Lågvatnet lake (1448 m a.s.l.) several defined moraine ridges cross the valley floor in the Jori river valley. These ridges, together with the marked lateral moraine along the western and eastern valley side of the Jori river valley at 1420 m a.s.l., show that a glacier dammed the Jori river valley in the southern part and a glacial lake was formed. This lake was drained through the run-off pass between the mountains of Skulan and Drugshøi into the upper parts of the Åmotdalen valley (Follestad 2011). Here, a set of well defined meltwater channels can be seen at 1380 m a.s.l. The glaciofluvial sand and gravel deposits west of Lågvatnet, situated at 1383 m a.s.l., support the idea of a glacial lake in the area (Figure 18).

In the Langvatn area (1411 m a.s.l.) lateral moraines are seen at both ends of the lake (Figure 18). The morphology of these lateral moraines show that they were formed by two separated glaciers entering the Langvatn lake area, from the west and the east. The lateral moraines along the western valley side of Larseggen mountain (1945 m a.s.l.) can be followed up to some 1500 m a.s.l. The lateral moraines seen along the northern mountainside of Drugshøi mountain support the existence of such a glacier.

The marked lateral moraine in the western parts of the Langvatn lake (1411 m a.s.l.) together with lateral moraines further down towards the southwest, show the existence of at least two

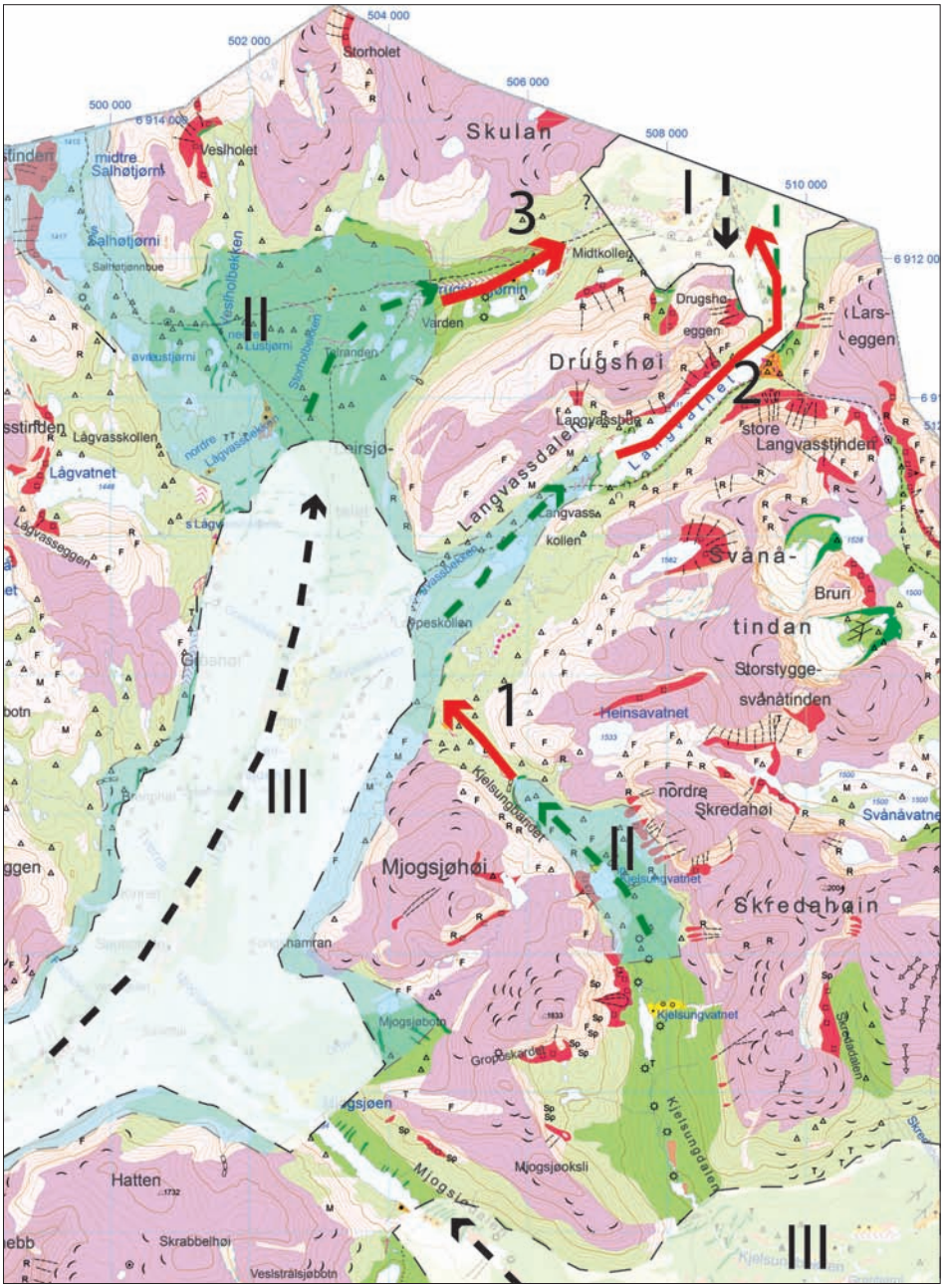

Figure 19. A tentative reconstruction of the development of glacier surfaces in the Jori river valley. Glaciofluvial run-off directions are shown with red arrows. Roman numerals are tentatively used to indicate a sequence of events.

glacier surfaces at some 1420 m a.s.l. and 1400 m a.s.l., respectively. The distinct end moraine in the area of Kjelsungbandet valley (between the mountains of Mjogsjøhøi and Svånåtindan) together with the glaciofluvial deposits in the areas to the west, support a glaciofluvial drainage in this direction after the formation of the upper marginal moraine in the Langvatn area, but before the formation of the lower lateral moraines in these areas (Figure 18). It should here be noticed that the Langvatn lake has marked shorelines 5–6 m above the present water level (1411 m a.s.l.). In the northern parts of lake 1415 m a.s.l. north of the Langvatn lake there is a well defined run-off pass, some 1417 m a.s.l. Thus it is likely that the northern parts of the Langvaten lake and the small lake 1415 m a.s.l. were glacier free when the shoreline formation and drainage in the northern areas occurred. This leads to the conclusion that the formation of the lateral moraine in the western end of the Langvatnet lake succeeded the formation of the lateral moraines in the northern parts of the lake.

Summarising discussion

Based on the description above a tentative glacial reconstruction is carried out (Figure 19). In the areas of the Langvatn lake it is concluded that these areas were ice free when glaciofluvial drainage (3) took place over the run-off pass in the north. Furthermore it is suggested that the glaciofluvial drainage (1) from the glacier represented by the lateral moraine in the Kjelsungbandet most likely was older or simultaneous with a glacier (marked in blue) depositing the lateral moraine in the western area of

lake Langvatnet. An ice surface at about 1420 m a.s.l. at at the western end of lake Langvatnet thus gives a glacier surface of about 1450 m a.s.l. in the areas along the west side of the Drugshøi mountain. Such a glacier surface is in agreement with the formation of the lateral moraines in the valley side of Skulan mountain and the glaciofluvial drainage pattern (3) to the northeast to the Åmotdalen valley. Somewhat later, the lower lateral moraines along the western valley side of the Jori river valley indicate that younger branches of glacier existed in the area (II). The drainage from the uppermost ice surface went eastward (3) to Åmotdalen. This drainage is also demonstrated by glaciofluvial accumulations at this altitude along the western side of the Jori river valley.

The marked Rogen moraines in the valley south of Mjogsjøhøi mountain indicate that deglaciation took place in a southeasterly direction and might be connected to the lower lateral moraines seen in the areas towards Hjerkinn. The higher lying lateral moraines in the southwestern side of the Mjogsjøhøi are thus considered to have formed more or less simultaneously with the highest lateral moraines in the areas to the north, along the Skulan mountain and in the western end of the Langvatn lake.

Glaciation limits in the investigated area

The glaciation limit represents the lowest altitude of a mountain at which glaciers can originate (Enquist 1916). In the western and northern parts of the Møre and Romsdal County cirque and small glacial valleys dominates. Here, well defined terminal moraines in some of the cirques show unequivocal evidence of cirque glaciation. Together with this information the present cirque glacier and the closest lying 'plateau peaks' are shown in Table 1.

In the Sunndalsøra (1420 II) area, Table 1 shows a glaciation limit at about 1685 m a.s.l. (as a mean of cirque 1, 5, 4 and 8) during the final parts of the glaciation. Corrected for the isostatic rebound from at the end of YD (~200 m) this gives a tentative glaciation limit of about 1485 m a.s.l. In the areas of Eresfjord (1320 II) the distribution of the terminal moraines give evidence for a glaciation limit at about 1230 m a.s.l. (as a mean of cirque 17, 19, 20, 21, 24, 26, 28, 29, 30, 31, 32, 34, 35, 36, 39 and 42) during the final parts of the glaciation. Corrected for the shoreline displacement at the end of YD (some 150 m) this indicates a tentative glaciation limit of some 1080 m a.s.l. Compared to the estimates of the modern glaciation limit for the eastern and western parts of the area (Østrem et al. 1988) at about 1800 m a.s.l. and 1450 m a.s.l., respectively, this suggests a general lowering of the glaciation limit in the YD of 350–370 m. Compared to the estimates for the YD depression of 400–500 m in the middle and inner Nordfjord (Fareth 1987) the calculated values in Møre and Romsdal County might be reasonable. It should be remembered that calculation of the YD glaciation limit in this paper is carried out using a 1 km grid on a map sheet. In Andersen (1968) the glaciated mountains are expected to lie at higher altitudes than the values received through use of the summit method. According to the map presented by Østrem et al. (1988), the modern glaciation limit rises from 1500 m a.s.l. to 1900 m a.s.l. over a distance of 60 km in a southeastern direction in the county of Møre and Romsdal. This gives a gradient of 6–7 m km^{-1} for the present glaciation limit.

Summary and discussion

Garnes and Bergersen (1980) and Bergersen and Garnes (1981) have, through detailed field mapping of lateral landforms, striae, texture and till fabric, reconstructed five deglaciation phases in the east Jotunheimen/Gudbrandsdalen area. During the final phases, called the 'C' and the 'D' phases, they found that the ice movements were to the north ('C') and to the northeast ('D') in areas north of the Otta valley. These observations are supported by the observation of northeasterly ice-flow configurations in east-central Norway and Sør-Trøndelag County, which are described by Follestad and Fredin (2007). In the following 'D' phase (Garnes and Bergersen 1980), the ice-directed meltwater drainage was to the northeast in the areas north of the Otta valley. This direction is confirmed by mapping of the drainage features on the Otta Quaternary map, scale 1:50,000, by Follestad and Bergstrøm (2004). According to these authors, the first recognised glaciofluvial drainage took place through the Vasskjelet run-off pass. This run-off pass is situated at 1520 m a.s.l., and is situated in the lower parts of the weathering material preserved on the west-facing slopes of Gråhøi mountain (1646 m a.s.l.). Even though this drainage landform in the Vasskjelet run-off pass is situated several tens of metres below the stipulated surface of an inland ice extrapolated from lateral moraine in the Raumadalen/Gudbrandsdalen area (Figure 9) it supports the view of a high-lying surface for the inland ice in the area of the Rondane mountain. Reconstructions made of the inland YD ice surface of Sollid and Kristiansen (1984) strongly support this view.

In the Littledalen valley west of Sunndalsøra, ^{14}C dating of shells gives a chronology for formation of the ice marginal deposits to some 9700 BP (Follestad 1987). This deposit, together with probably contemporary lateral moraines in the Reinsvatnet lake and in the Skarvdalen valley is evidence for a high-lying ice surface in the Aursjøen area. The ice sheet surface in the Littledalen–Aursjøen valley and the Eikesdalen–Aursjøen valley, together with the surface of the inland ice in the Rauma–Lordalen valley, can be followed up to 1540 m a.s.l. and 1560 m a.s.l., respectively. In the profile (Figure 17) gradients for the inland surface are stipulated to some 26 m km^{-1}. Extrapolations in an eastward direction will give a tentative surface for the

Table 1. Mountain peak, the orientation of the cirque or cirque valleys with or without terminal moraines. The present-day cirque glaciers are indicated.

Sample no	m a.s.l.	Cirque orientation	Terminal moraines	Cirque glacier today (x)
Map sheet: Sunndalsøra 1420 III				
1 Vardefjell	1686	East (E)	X	-
2 Slotthø	1833	North (N)	X	X
3 Midtfonntinda	1707-17950	N	X	X
4 Austvindstrøe	1660	E	X	X
5 Vikesaksa	1809	E	X	-
6 Såtatind	1614	N	X	X
7 Breidtelnebba	1735	N	X	-
8 Topp 1512	1512	N	X	-
9 Ryssdalsnebba	1818	E	X	X
10 Gråfjell	1264	E	X	-
11 Skjorta	1711	E	X	X
12 Topp 1292	1292	South (S)	X	-
13 Trolltind	1396	E	X	X
14 Hjellbønebba	1557	-		-
15 Skrondalsnebba	1463	E	X	-
16 Kleppen	1535	-		-
Map sheet: Eresfjord 1320 II				
17 Nyheitind (i)	1508	N	X	-
18 Nyheitind (ii)	1598	N	X	X
19 Høgseternebba	1241	N	X	-
20 Helvetestind	1373	N	X	-
21 Storbrefjellet	1287-1340	E	X	-
22 Storbreen	1524-1470	E	X	X
23 Topp 1616	1616	E	X	X
24 Blåfjellet (i)	1276	E	X	-
25 Store Vengjetind	1852	E	X	X
26 Kyrkjetaket	1439	E	X	-
27 Klauva (i)	1512	N	X	X
28 Blåfjellet (ii)	1162	E	X	-
29 Kalvgjeltind	1283	West(W)	X	-
30 Snarketind	1149	N	X	-
31Svartevasstind	1160	N	X	-
32 Blånebbå	1320	E	X	-
33 Bjørnabotnhøgda	1470	N	X	X
34 Topp 1324	1324	N	X	-
35 Måsvasstind	1203	N	X	-
36 Såta	1131	N	X	-
37 Nebba	1105	-	-	-
38 Skrokkenfjellet	1057	-	-	-
39 Ryptind	943	E	X	-
40 Dølmørhaugen	1000	E	X	-
41 Nebbeslia	893	-	-	-
42 Langbotn	1100	E	X	-
43 Blåfjellet (iii)	1154	-		-

inland ice at 1700–1800 m a.s.l. in the Dombås area. The lateral moraines can be followed up to 1540 m a.s.l. in the Aursjøen area and to 1560 m a.s.l. in the Storhøe area north of Lesja (Follestad 2010). These numbers might give an indication of the equilibrium line altitude during this time period, and the formation of these deposits at altitudes of 1540–1560 m, or 1340–1360 m, if corrected for the shore displacement. These numbers seem to be acceptable for the general lowering of the snowline in YD compared to the lowering described elsewhere in the country, e.g., in the Nordfjord area (Fareth 1987).

In the till sequences presented by Garnes and Bergersen (1980) there is no evidence for lowering and then regeneration of the ice sheet surface to an altitude of 1700–1800 m in the Dombås area. This implies that the latest ice culmination was in the Jotunheimen mountains with outlet glaciers flowing through the valleys of Lordalen and Grøndalen. This took place before and during the formation of the upper set of YD lateral moraines deposited in the Rauma–Gudbrandsdalen area as well as in the Aursjøen–Littledalen area. The lower set of lateral moraines observed in the Raumadalen–Gudbrandsdalen areas might represent a still-stand or a readvance during the deglaciation. Similar situations are described in the Oppdal–Hjerkinn area. These lateral moraines are here correlated to the readvances in Sør-Trøndelag County (Follestad 2003), dated to late YD chronozone, some 10,300–10,400 ^{14}C years BP (Sollid and Reite 1983).

In Figures 16 and 17 the ice surfaces are used and extrapolated in an eastward direction. If the lowest obtained gradient of 13 m km^{-1} is used, then an altitude of 1750 m a.s.l. for the ice surface is likely in the Dombås–Fokstugumyra area and about 2000 m a.s.l. in the Rondane area. However, as we approach the culmination zone of the ice sheet south of the Rondane mountain in the Ringebu areas (Garnes and Bergersen 1980), the slope gradient might have been considerable lower, as indicated in Figure 16. In this case, using a slope gradient of 5 m km^{-1}, the projected ice-sheet surface will be at about 1600 and 1750 m a.s.l. in the areas of Dombås–Fokstugumyra and Rondane, respectively. Furthermore, the ice divide in the Ringebu areas must have existed for a significant period, as the following meltwater drainage was to the north and northeast (Follestad and Bergstrøm 2004, Follestad 2005). An ice-sheet surface of 1750–2000 m in the Rondane mountains is also consistent with the ice-flow directions indicated by the drumlins in the Fokstugumyra area (Follestad and Fredin 2007).

Conclusions

The lateral moraines in the area of Romsdalen–Gudbrandsdalen valley and in the valleys of Aursjøen–Littledalen/Eikesdalen form a pattern reflecting ice-sheet surfaces at about 1540 m a.s.l. and 1560 m a.s.l., respectively. The slope gradients for the inland ice surface for the upper and lower marginal zones are deduced to 13 m km^{-1} in the main valley of Gudbrandsdalen. This will give a tentative maximum ice surface at 2000–1750 m a.s.l. for the two marginal zones described in the Dombås and Fokstugumyr areas. This leads to the conclusion that the Rondane mountains and surrounding areas were covered by ice or acted as accumulation area nunataks; however, nunataks and ice-free areas probably existed in high-altitude areas during the YD chronozone. Thus, the ice-sheet geometry, deduced from lateral moraines, supports 'a thick-ice model' for the Upper (late) Weichselian Scandinavian ice sheet in Norway, where much of the core areas are inundated by ice. Furthermore it is suggested that continuous melting of the inland ice took place from the Late glacial maximum to the YD chronozone and that the main ice divide was situated in the Jotunheimen mountain, from where major ice streams emanated into the field area.

Acknowledgements

Financial support for this study was given by the Geological Survey of Norway and Lesja Municipality and is acknowledged with thanks. We would like to thank Lars Olsen and Jochen Knies for their critical and constructive comments on an earlier version of the manuscript. Bjørn-Ivar Rindstad helped extract relevant landforms from the Geological Survey of Norway databases. Leif Sørbel kindly reviewed the manuscript, Journal Editor Trond Slagstad offered valuable comments on the manuscript and the English was corrected by Paul McCormic. The authors would like to express their gratitude to these colleagues and other persons who have contributed in different ways.

References

Andersen, B.G. (1954) Randmorener i Sørvest-Norge. *Norwegian Journal of Geography*, **14**, 274–342.

Andersen, B.G. (1960) Sørlandet i Sen- og Postglacial tid. *Norges geologiske undersøkelse*, **210**, 142 pp.

Andersen, B.G. (1981) Late Weichselian ice sheet in Eurasia. Greenland and Norway. *In* Denton, G. and Hughes, T.J. (eds.) *The Last Great Ice Sheets*, Wiley, New York, pp. 20–27.

Andersen, B.G. (2000) *Istider i Norge*, Universitetsforlaget, Oslo, 216 pp.

Andersen, B.G., Lundquist, J. and Saarnisto, M. (1995) The Younger Dryas margin of the Scandinavian ice sheet–an introduction. *Quaternary International*, **28**, 145–146 .

Anundsen, K. (1972) Glacial chronology in parts of south-western Norway. *Norges geologiske undersøkelse*, **280**, 1–24.

Benn, D.I. and Evans, D.J. (1998) *Glaciers and Glaciation*, Hodder Arnold, London, 734 pp.

Bergersen, O.F. and Garnes, K. (1981) Weichsel in central South-Norway: the Gudbrandsdalen interstadial and the following ice ages. *Boreas*, **10**, 315–322.

Bergersen, O.F. and Garnes, K (1983) Glacial deposits in the culmination zone of the Scandinavian ice sheet. *In* Ehlers, J. (ed.) *Glacial deposits in north-west Europe*, Balkema, Rotterdam, pp. 23–40.

Bonow, J.M., Lidmar-Bergström, K. and Näslund, J.O. (2003) Palaeosurfaces and major valleys in the area of the Kjølen mountains, southern Norway–consequences of uplift and climatic change. *Norwegian Journal of Geography*, **57**, 83–101.

Boulton, G.S., Smith, G.D., Jones, A.S. and Newsome, J. (1985) Glacial geology and glaciology of the last midlatitude ice sheet. *Journal of the Geological Society of London*, **142**, 447–474.

Dahl, S.O., Nesje, A. and Øvstedal. J. (1997) Cirque glaciers as morphological evidence for a thin Younger Dryas ice sheet in east-central southern Norway. *Boreas*, **26**, 161–180.

Ebbing, J. and Olesen, O. (2005) The Northern and Southern Scandes–structural differences revealed by an analysis of gravity anomalies, the geoid and regional isostasy. *Tectonophysics*, **411**, 73–87.

Enquist, F. (1916) Der einfluss des Windes auf der verteilung der Gletscher. *Bulletin of the Geological Institution of the University of Upsala*, **14**, 1–108.

Fareth, O.W. (1987) Glacial geology in middle and inner Nordfjord, western Norway. *Norges geologiske undersøkelse Bulletin*, **408**, 1–55 pp.

Follestad, B.A. (1972) The deglaciation of the south-western part of the Folgefonn Peninsula, Hordaland. *Norges geologiske undersøkelse*, **280**, 31–64.

Follestad, B.A. (1987) Sunndalsøra 1420 III. Beskrivelse til kvartærgeologisk kart–M 1:50,000. *Norges geologiske undersøkelse Skrifter*, **79**, 32 pp.

Follestad, B.A. (1994) Nesset Kommune. Kvartærgeologisk kart–M 1:80,0000. Tema: Jordarter. *Norges geologiske undersøkelse*.

Follestad, B.A. (2003) Development of minor late-glacial ice domes east of Oppdal, Central Norway. *Norges geologiske undersøkelse Bulletin*, **441**, 39–49.

Follestad, B.A. (2005) Rondane, Quaternary geology map 1718 I, scale 1:50,000, *Norges geologiske undersøkelse*.

Follestad, B.A. (2006) Dombås, Quaternary geology map 1419 II, scale 1:50,000, *Norges geologiske undersøkelse*.

Follestad, B.A. (2008) Lesjaskog, Quaternary geology map 1419 III, scale 1:50,000, *Norges geologiske undersøkelse*.

Follestad, B.A. (2010) Lesja Municipality, Quaternary geology map, scale 1:80,000, *Norges geologiske undersøkelse*.

Follestad, B.A. and Bergstrøm, B. (2004) Otta, Quaternary geology map 1718 IV, scale 1:50,000, *Norges geologiske undersøkelse*.

Follestad, B.A. and Fredin, O. (2007) Late Weichselian ice flow evolution in south-central Norway. *Norwegian Journal of Geology*, **87**, 281–289.

Follestad, B.A., Larsen, E., Blikra, H., Longva, O., Anda, E., Sønstegaard, E., Reite, A. and Aa, A.R. (1994) Løsmassekart over Møre og Romsdal fylke–Beskrivelse. *Norges geologiske undersøkelse Skrifter*, **112**, 52 pp.

Garnes, K. and Bergersen, O.F. (1980) Wastage features of the inland ice sheet in central South-Norway. *Boreas*, **9**, 251–269.

Kleman, J. and Hättestrand, C. (1999) Frozen-bed Fennoscandian and Laurentide ice sheets during the last glacial maximum. *Natur*e, **402**, 63–66.

Mangerud, J. (2004) Ice sheet limits on Norway and the Norwegian continental shelf. *In* Ehlers, J. and Gibbard, P. (eds.) *Quaternary Glaciations–Extent and Chronology. Volume 1 Europe*, Elsevier, Amsterdam, pp. 271–294.

Mangerud, J., Gyllencreutz, R., Lohne, Ø. and Svendsen, J.I. (2011) Glacial history of Norway. *In* Ehlers, J., Gibbard, P.L. and Hughes, P.D. (eds.) *Quaternary Glaciations - Extent and Chronology*. Elsevier, Europe, Amsterdam, pp. 279-298.

Nesje, A., Dahl, S.O., Anda, E., and Rye, N. (1988) Block fields in southern Norway, significance for the Late Weichselian ice sheet. *Norsk Geologisk Tidskrift*, **86**, 149–169.

Paus, Aa., Gaute, V., Larsen, J., Nesje, A. and Lie, Ø. (2006) Late glacial nunataks in central Scandinavia: Biostratigraphical evidence for ice thickness form Lake Flåfattjønn, Tynset, Norway. *Quaternary Science Reviews*, **25**, 1228–1246.

Reite, A. (1990) Sør-Trøndelag County. Quaternary geology map, scale 1:250,000, Map description. *Norges geologiske undersøkelse Skrifter*, **96**, 1–39.

Reite, A. (1994) Weichselian and Holocene geology of Sør-Trøndelag and adjacent parts of Nord-Trøndelag County, Central Norway. *Norges geologiske undersøkelse Bulletin*, **426**, 1–30.

Sollid, J.L. and Kristiansen, K. (1984) Raumavassdraget, kvartærgeologi og geomorfologi, scale 1:80,000. Geografisk institutt, Universitetet i Oslo.

Sollid, J.L. and Reite, A. (1983) The last glaciation and deglaciation of Central Norway. *In* Ehlers, J. (ed.) *Glacial deposits in north-west Europe*, A.A. Balkema, Rotterdam, pp. 41–60.

Stroeven, A.P., Fabel, D., Harbor, J., Hättestrand, C., and Kleman, J. (2002) Quantifying the erosional impact of the Fennoscandian ice sheet in the Torneträsk–Narvik corridor, northern Sweden, based on cosmogenic radionuclide data. *Geografiska Annaler*, **84A**, 275–287.

Vorren,T.O. (1973) Glacial geology of the area between Jostedalsbreen and Joutunheimen. *Norges geologiske undersøkelse*, **291**, 46 pp.

Vorren, T.O. (1977) Weichselian ice movement in South Norway and adjacent areas. *Boreas*, **6**, 247–257.

Undås, I. (1963) *Ra-morenen i Vest-Norge*, Eides Forlag A/S, Bergen. 40 pp.

Østrem, G., Selvig, K.D. and Tandberg, K. (1988) Atlas over breer i Sør-Norge. *Hydrologisk avdeling, Norges vassdrags- og energiverk*, Meddelse nr 61.

RESEARCH ARTICLE

Temperature footprint of a thermal response test can help to reveal thermogeological information

Heiko T. Liebel[1,*], Kilian Huber[2], Bjørn S. Frengstad[3], Randi K. Ramstad[4], Bjørge Brattli[1]

[1] Norwegian University of Science and Technology, Department of Geology and Mineral Resources Engineering, 7491 Trondheim, Norway
[2] University of Bayreuth, Department of Geology, Universitätsstr. 30, 95440 Bayreuth, Germany
[3] Geological Survey of Norway, P.O.Box 6315 Sluppen, 7491 Trondheim, Norway
[4] Asplan Viak AS, Postbox 6723, 7490 Trondheim, Norway
**heiko.liebel@ntnu.no*

Borehole heat exchangers connected to a ground-coupled heat pump extract heat from the ground for the heating of buildings. Heat is transferred to the ground in cooling mode and can be extracted again during the next heating season. To dimension a large borehole field designed to meet the heating and cooling demand of a building, important ground parameters (temperature, volumetric heat capacity of the rocks, thermal conductivity, thermal borehole resistance) are needed. One important parameter is the effective thermal conductivity, which is measured with the help of thermal response tests (TRT). A temperature profile is measured before a TRT to find the undisturbed ground temperature. Rarely, temperature profiles are also measured after a finished TRT. Experience from about twenty TRTs shows, however, that important hydro- and thermogeological characteristics of the borehole may affect the measured ground parameters. These can be detected from temperature profiles after the TRT. Measuring the temperature profile in a well after a TRT can add valuable information to the study and about the nature of a borehole heat exchanger system. Four typical cases are discussed: a standard case of a borehole drilled in homogeneous and non-fractured rocks without any temperature anomaly and three more complicated cases, involving heat loss from buildings, groundwater flow through a single fracture and groundwater up-flow through the borehole from a confined artesian aquifer. Extra information about groundwater flow, open fractures and varying mineral content in the rocks can help to evaluate the TRT results and to suggest a better design of a ground-coupled heat pump installation. Based on the results of our study it is highly recommended to take temperature profiles after TRTs.

Liebel, H.T., Huber, K., Frengstad, B.S., Ramstad, R.K. and Brattli, B. (2011) Temperature footprint of a thermal response test can help to reveal thermogeological information. *Norges geologiske undersøkelse Bulletin*, **451**, 20–31.

Introduction

Geothermal energy is most often understood as heat that is accessible from the Earth's crust. This heat is mainly produced from radioactive decay of minerals but may also include residual heat from the formation of the Earth. Geothermal energy is used for electricity production in areas with an unusually high geothermal gradient (e.g., Iceland, Indonesia, Italy). These areas are mostly restricted to plate boundaries where heat is transported towards the Earth's surface via conductive and convective heat flow. A low-temperature variant of geothermal energy can be used, however, in most places and most effectively in regions with seasonal climate for the heating and cooling of buildings. In this case the energy is not generated in the ground but predominantly stored and renewed with the help of solar irradiation. A term frequently used to distinguish the heat source from pure geothermal heat is 'ground-source heat'. This term may be misleading as the main heat source is not the ground (e.g., average annual geothermal heat flux in Sweden: 0.6 kWh m^{-2}, Andersson 2011). The ground is predominantly a storage medium for the solar irradiative heat (e.g., average annual solar heat flux towards the ground in Sweden: 1500 kWh m^{-2}, Andersson 2011). Therefore, a more precise term should be used: 'ground-stored heat'.

To extract this ground-stored heat, borehole heat exchangers (PE collectors, mostly U-shaped in Scandinavia) are installed in shallow boreholes. A heat-carrier fluid circulates through the borehole heat exchanger and delivers heat to a ground-coupled heat pump which transfers the energy to the building in heating mode. In heating mode heat is removed from the rock. After a considerable removal of heat, a significant heat flow from the surface is established (Figure 1).

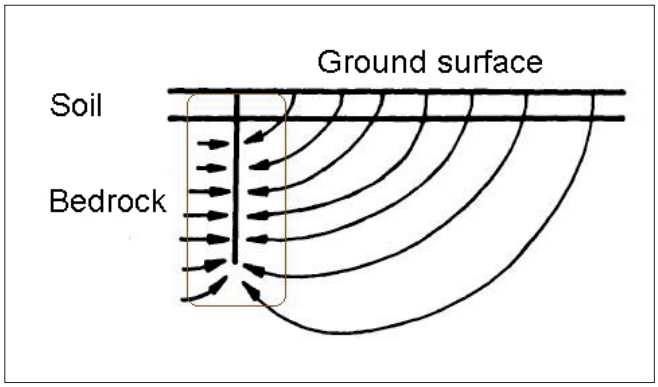

Figure 1. Energy refill around a shallow borehole from solar radiation under stationary conditions (minor geothermal refill is neglected in the figure; Nordell 2008, mod.).

Most commercial buildings have also a need for cooling in the warm season. This applies also to the Nordic countries because of the greenhouse effect of buildings with extensive glass facades or the heat production from computers and other electrical equipment. To satisfy the cooling needs, the heat pump can be reversed and heat can be transferred to the ground. This heat is then available to be brought up again in the next heating period. In this case waste energy is stored in the ground.

Ground-coupled heat pumps are used widely in single houses with a few wells and in commercial buildings or interconnected housing areas with up to 8006 boreholes like in Fort Polk (Louisiana, Hughes 2001). The largest well field in Europe until now is installed at Akershus University Hospital (Norway). There, 228 wells were drilled and furnished with borehole heat exchangers. About 40% of the building's heat load (ca. 20 GWh per year) is expected to be covered with energy mostly from ground-coupled heat pumps (www.fornybar.no, 11.04.2011).

The capacity of ground-coupled heat pumps worldwide has increased from around 1 800 MW (thermal) in 1995 to around 15 000 MW (thermal) in 2005 (Lund et al. 2005) and 35 000 MW (thermal) in 2010 (Lund et al. 2010). The market for ground-coupled heat pumps is also forced to increase in many countries as the use of renewable energy for heating and cooling of buildings is regulated by law. In new buildings in Norway, for example, technical regulation TEK07, § 8–22, requires that after 2007, 40% of the energy required for space and domestic water heating has to be delivered by other energy sources than electricity or fossil fuels.

The decision about how many metres of borehole have to be drilled to meet the heating or cooling load of a building is crucial for the successful and long-lived operation of the ground-coupled heat pump. The needed borehole length can be calculated if the thermal ground and well properties are known. Important parameters are temperature of the rock, volumetric heat capacity, thermal borehole resistance and effective thermal conductivity at a site. The knowledge of them will help to find a good compromise between costs (drilling and operation costs to run the ground-coupled heat pump system) and efficiency (supplying expected heat and cold loads). Thermal borehole resistance and effective thermal conductivity are measured with the help of a thermal response test (TRT, see Austin 1998 and Gehlin 1998). TRTs are applied as a standard procedure before a large well field is dimensioned and the results are considered to be essential for the proper dimensioning.

The objective of this study is to show the importance of temperature profiles before and after TRTs for the interpretation of the TRT results.

Before each TRT, a temperature profile is measured to find the undisturbed ground temperature which is a necessary parameter for the determination of the thermal borehole resistance (e.g., Gehlin 1998). Less attention, however, has been given so far to measure temperature profiles after a TRT. Experience from around 20 TRTs, with temperature profiles taken before and after TRTs, gives us an overview over the most common phenomena that can be observed. The temperature profiles can be grouped into four cases. Four illustrative examples are chosen

where observed temperature variations and their implication on the TRT evaluation are discussed.

Materials and methods

Thermal response test

Thermal response tests are often applied in Scandinavia and many countries worldwide to evaluate the in situ or effective thermal conductivity in a borehole. For this purpose the TRT equipment is connected to the borehole heat exchanger of the energy well (PE collector pipes, most commonly U-shaped, see Figure 2).

Heating elements in a portable TRT trailer warm up the heat-carrier fluid that is circulating through the closed-loop system. The connection between the trailer and the borehole has to be well insulated, to avoid heat loss in cold weather or heat gain through sun irradiation. The circulation pump creates a turbulent flow in the pipes to get best heat transport from the collector towards the ground. The undisturbed ground temperature (measured before the TRT) and the temperature increase in the heat-carrier fluid during a test run are used to calculate the effective thermal conductivity of the ground (λ_{eff}) and the borehole thermal resistance (R_b). λ_{eff} is a parameter which integrates a) the ability of the bedrock surrounding the borehole to conduct heat (Fourier's law), b) buoyancy-driven convection in the borehole due to the heat input along the collector tubes (e.g., Gustafsson et al. 2010), and c) groundwater movement in or in the vicinity of the borehole (e.g., Gehlin et al. 2003).

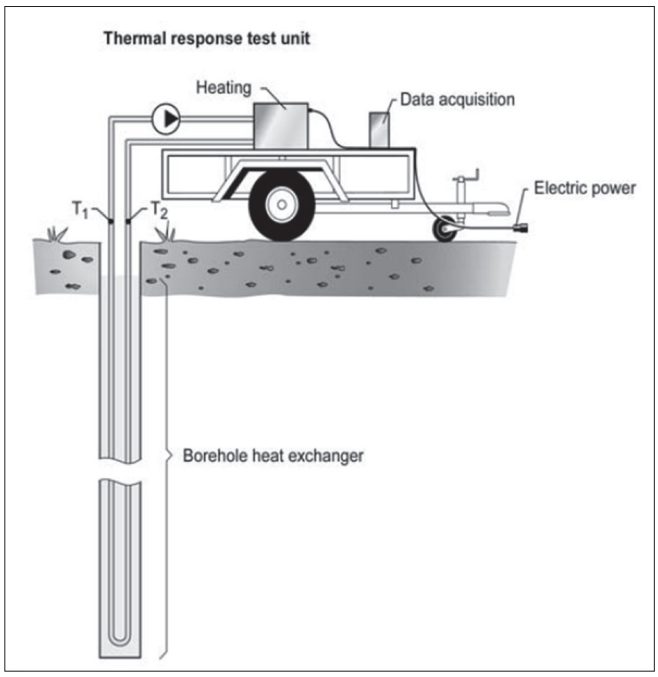

Figure 2. TRT rig connected to a borehole heat exchanger (Gehlin 2002).

The calculation of λ_{eff} follows the suggestions of Gehlin (2002) and Signorelli et al. (2007), which are based on the infinite line-source theory (Ingersoll 1948). The line-source model is based on a linear relationship between the average heat-carrier fluid in the collector and the natural logarithm of the time t, if the heat exchange rate per length unit, q, is constant (q is constant if the electric power supply to the heating elements is constant):

$$T_f(t) = k \ln(t) + m \quad [\mathrm{K}] \qquad (1)$$

where

$$k = \frac{q}{4\pi\lambda} \quad [\mathrm{K}] \qquad (2)$$

and

$$m = q\left[R_b + \frac{1}{4\pi\lambda}\left(\ln\left(\frac{4\lambda}{r_b^2 S_{VC}}\right) - 0.5722\right)\right] + T_0 \quad [\mathrm{K}] \qquad (3)$$

r_b is the borehole radius, S_{VC} is the volumetric heat capacity of the rock/sediment, and T_0 is the undisturbed ground temperature. The average heat carrier-fluid temperature, T_f, is calculated from the inlet and outlet temperatures, T_{in} and T_{out}:

$$T_f = \frac{T_{out} + T_{in}}{2} \quad [\mathrm{K}] \qquad (4)$$

The thermal conductivity λ is found by plotting T_f against the natural logarithm of the time in seconds and by reading off the slope where the conditions have stabilized (e.g., Signorelli et al. 2007; normally between 20 (t_1) and 70 hours (t_2)):

$$\lambda = \frac{q}{4\pi} \cdot \frac{\ln(t_2) - \ln(t_1)}{T_f(t_2) - T_f(t_1)} \quad [\mathrm{W\ m^{-1}\ K^{-1}}] \qquad (5)$$

A TRT typically lasts 72 hours (Gehlin 1998). In this time range the analytical solution of the infinite line-source shows a very low error level compared to the alternative solutions of the finite line-source and the infinite cylindrical-source theory (Philippe et al. 2009). Different international guidelines recommend durations of at least 36 hours (IGSHPA) or 50 hours (IEA). In Germany, commonly a TRT is considered to be long enough if the estimated effective thermal conductivity does not change more than 0.1 W $m^{-1}K^{-1}$ within 24 hours (M. Sauer, pers. comm. 2011).

In case of strong groundwater flow through the borehole, the parameters of interest (in our case: λ_{eff}) can be approximated with a parameter estimation technique which varies the unknown variables in equations 1–3 to find the best fit between calculated and measured data for time-varying heat inputs (see also Shonder and Beck 1999, Wagner and Clauser 2005, Witte 2007).

Possible sources of error during a TRT are: 1) heat loss and gain (affects T_f), 2) variable electric power supply (affects q),

3) accuracy of the determination of the undisturbed ground temperature (affects T_0), 4) free convection of water in non-grouted boreholes (standard for energy wells in Scandinavia; affects λ; Gustafsson et al. 2010), 5) gradient-driven horizontal groundwater flow (affects λ; e.g., Gehlin and Hellström 2003) and 6) density-driven vertical groundwater flow (affects λ; e.g., thermosiphon effect, Gehlin et al. 2003, Gustafsson 2006, Gustafsson and Westerlund 2010). Typical levels of confidence of TRT results are about 9% for the thermal conductivity (Zervantonakis and Reuss 2006). If thermo- or hydrogeological situations are present that alter the effective thermal conductivity measurement, temperature profiles help to interpret the obtained TRT data or help to detect the special situation.

Temperature profiles

Temperature profiles were taken directly in one shank of the single U-shaped borehole heat exchanger before each TRT to determine the undisturbed ground temperature, T_0, and four to five hours after the end of the TRT. The local heat flux is the product of thermal conductivity and temperature gradient (Fourier's law of heat conduction). The heat flux is strongest in areas where the temperature decreased most during the recovery time after the TRT. In these areas a high effective thermal conductivity can be expected due to high thermal conductivity of the bedrock or due to groundwater flow.

The depth interval was two or four metres. It is necessary to keep the measurement time of a temperature profile short to avoid a further temperature recovery during the measurement after a TRT. Measuring a temperature profile for a 200 m long borehole took about 70 minutes. The temperature recovery during the temperature measurement depends on the heat input during the TRT and the thermal properties of the borehole and the surrounding bedrock (see also Javed et al. 2011). In a study recently presented (Liebel et al. 2011), the temperature recovery in a 138 m deep borehole was registered also after the TRT was finished. The temperature dropped within the first four hours by 2.6°C. Within the next hour the temperature decrease was 0.1°C only (heat input during the TRT: 3 kW for 94 hours). The temperature recovery is very fast in the first few hours before it slows down significantly. Therefore, four to five hours after a TRT seem to be a good timing for the temperature measurement after the TRT.

Fiber optic cables have recently been applied to observe temperature variations along the entire borehole (Fujii et al. 2009, Acuña and Palm 2010). They give very good control over temperature variations and temperature developments. However, their applicability is to date restricted to research due to the high costs of the analytical equipment. Therefore, economically attractive, ordinary temperature dataloggers are used in this study.

Results and discussion

Observations at the different sites

From a dataset of about 20 TRTs performed in Norway, four illustrative cases were chosen to be discussed in this study (see Figure 3).

All cases show phenomena that can be found frequently in temperature measurements related to TRTs and they have different implications on the evaluation of the TRT results. Some general data of the TRTs are presented in Table 1.

Fredrikstad

Outcrops close to the borehole in Fredrikstad show a rather homogeneous light reddish, biotite-bearing, medium-grained Iddefjord granite, which crystallised from magma in the Precambrian around 920–930 Ma ago (Pedersen and Maaloe 1990). The granite contains quartz, biotite, orthoclase, plagioclase, some muscovite and small amounts of apatite, titanite, magnetite and zircon (Holtedahl 1953) and it is interpreted as the continuation of the Bohus granite in Sweden. Outcrops around the borehole and information from the driller's well report indicate granite along the entire borehole length.

Regional fracture zones are present but show low hydraulic conductivity because of the appearance of swelling-clay minerals due to hydrothermal alterations and/or deep weathering in

Table 1. General data of the four TRTs presented in this study.

Location	Coordinates	Altitude m a.s.l.	Borehole depth (m)	Date of TRT	λ_{eff} (W m^{-1}K^{-1})	Duration of TRT (hr)
Fredrikstad	611848 E 6565630 N	17	200	26.07.–29.07.2009	3.15	72
Nordstrand	600555 E 6637162 N	130	200	06.07.–09.07.2009	3.23	65
Lade	572043 E 7037069 N	25	150	20.09.–04.10.2009	4.11	333
Bjørnegård	583691 E 6639799 N	6	200	26.08.–30.08.2010	4.81	95

Coordinates refer to UTM zone 32, WGS84.

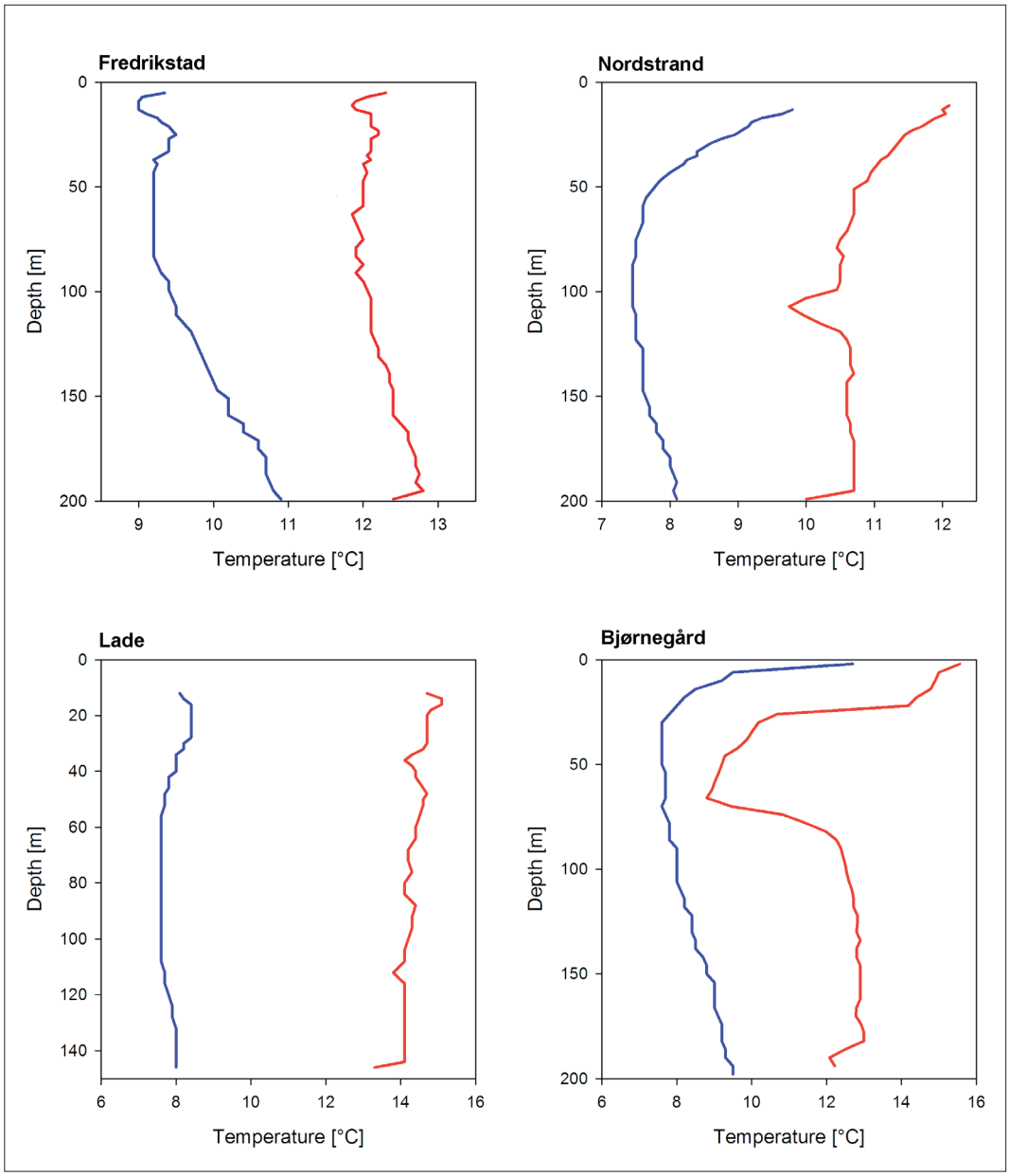

Figure 3. Temperature profiles before (blue) and after (red) a TRT at the four different study sites: Fredrikstad, Nordstrand, Lade and Bjørnegård.

the Triassic and Jurassic period (Banks et al. 1992a, b, 1994, Olesen et al. 2006).

Slagstad et al. (2009) measured a rock core thermal conductivity of 3.1 W $m^{-1}K^{-1}$ in the Iddefjord granite which is consistent with the TRT result: 3.15 W $m^{-1}K^{-1}$. The almost identical result indicates that the borehole is surrounded by granite only with negligible alteration of effective thermal conductivities due to groundwater flow. Also the temperature profile taken after the TRT supports this hypothesis (Figure 3). The uppermost ten metres of the borehole are influenced by seasonal variation while the following 60 m are influenced by (palaeo-) climatic effects as described by Slagstad et al. (2009), before a normal geothermal gradient is followed down to the base of the borehole.

The latter effects are most pronounced in the temperature profile before the TRT, but they are still detectable in the temperature profile after the TRT. The temperature profile shows no major variations along the borehole with the exception of a sudden temperature drop at the base. This effect can be explained with a stronger vertical heat flow at the bottom of the borehole due to heat flow from the sides and from below. As a consequence the cool-down is faster than in other parts of the borehole.

Nordstrand

The borehole used for the TRT at Nordstrand (borehole 3, see Figure 4) was drilled only two metres away from a large school building which dates back to the year 1926. Through the last 85 years, heat has been transferred from the building to the ground due to poor insulation.

The area around the investigated well field is dominated

by garnet-rich tonalitic gneisses, a few kilometres west of the Mysen syncline (1660–1500 Ma; Graversen 1984, Lutro and Nordgulen 2008).

Sheet silicates like biotite are a main component of the gneisses at Nordstrand. They are responsible for a strong anisotropy effect in their thermal conductivity. Clauser and Huenges (1995) investigated the thermal conductivity of biotite and measured 3.1 W $m^{-1}K^{-1}$ parallel to the sheets and 0.5 W $m^{-1}K^{-1}$ perpendicular to the sheets. The strike and dip direction is expected to vary along the borehole as outcrops showed folding in the gneisses.

At an outcrop approximately 50 m west of the well field, another local rock type was discovered: a felsic pegmatite dyke (about 2 m thick). It is expected that the dyke cuts the borehole so that both gneiss and pegmatite are present in the well.

The thermal conductivity of the gneiss is expected to be somewhat lower than that of the pegmatite. Values recommended to be used in Earth Energy Designer for gneiss and pegmatite are 2.9 and 3.4 W $m^{-1}K^{-1}$, respectively (Eskilson et al. 2000). In the GEOS (GEOlogy of the OSlo region) database of the Geological Survey of Norway a median value of 3.04 W $m^{-1}K^{-1}$ for the gneiss present at Nordstrand was calculated based on 91 surface rock core samples. The effective thermal conductivity measured with the TRT in this study is 3.23 W $m^{-1}K^{-1}$ and is within the expected range. The driller's well report indicates a water-bearing fracture zone at 110–112 m depth.

Two different phenomena can be discovered while studying the two different temperature profiles related to the TRT: 1) the thermal influence of buildings on the temperature field in the ground, and 2) the presence of groundwater flow at 34 m depth.

The temperature increase in the temperature profile taken before the TRT is remarkably high in the uppermost 60 m of the borehole (see Figure 3). Therefore, three additional temperature profiles were taken in surrounding boreholes 1, 2 and 4 (see Figure 5).

The thermal disturbance in the ground decreases proportionally to the increasing distance to the main building of Nordstrand school. The same phenomenon was described for a building in Cambridge (Massachusetts, USA) where the influence was modelled to be down to almost 150 m, 50 years after the construction of the building (Roy et al. 1972). Roy et al. modelled the underground heat plume defining a Dirichlet temperature boundary condition for the building which was set to 15°C. This strategy was taken in a simple two-dimensional finite-element model for the thermal plume at Nordstrand school. The model was built up in FEFLOW 5.4 (DHI–WASY GmbH, Berlin, Germany). Using a transient model with a thermal conductivity of 3.23 W $m^{-1}K^{-1}$, a matrix porosity of 5% (used as pseudoparameter), a geothermal gradient of 0.7 K per 100 m and a simulation time of 82 years (time since the building was built), the temperatures measured in the uppermost 100 m can be simulated successfully (see Figure 6 and compare also with Figure 5).

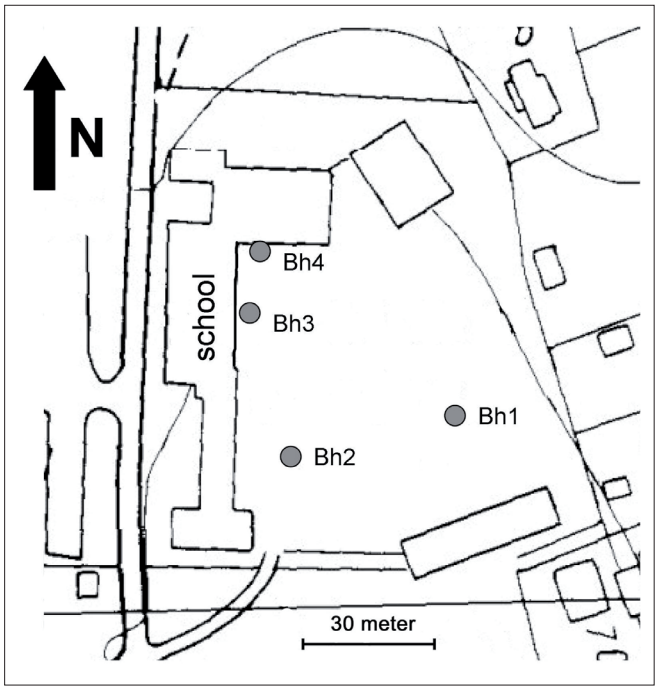

Figure 4. Map over Nordstrand school and position of boreholes (Bh) where temperature profiles were taken (map taken from www.norgeskart.no, 08.12.2009, mod.).

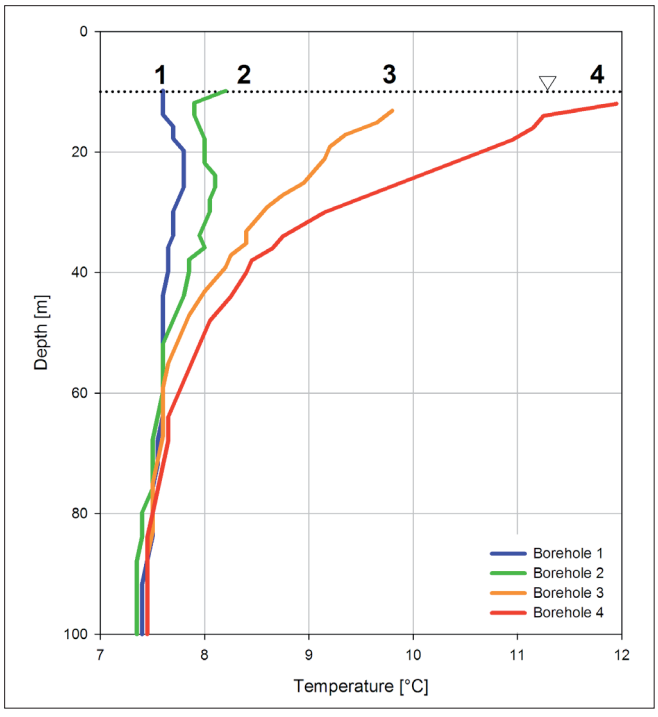

Figure 5. Temperature profiles in four boreholes at Nordstrand. The dotted line and the triangle show the groundwater level.

The heat loss through the foundations of the building over many years is significant and underlines the importance of good insulation.

Groundwater has an influence on the temperature recovery after the TRT. The driller's well report indicates a water-

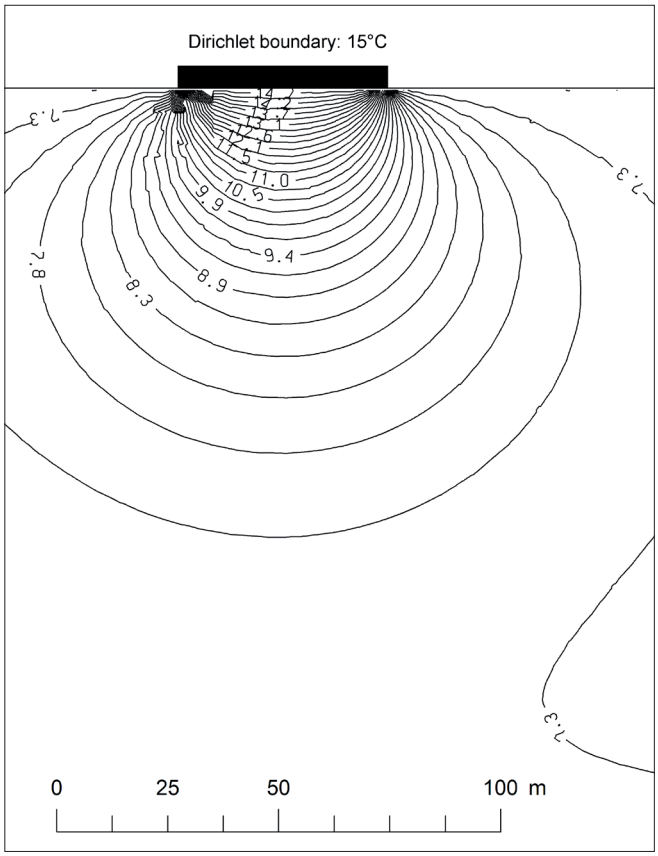

Figure 6. Simulated heat plume below Nordstrand school 82 years after the construction.

bearing fracture zone at 110 to 112 m depth and exactly there, the temperature decrease is fastest after the TRT. The effect of groundwater on the temperature profile was further investigated in a research borehole of the Geological Survey of Norway at Lade (see discussion below).

Lade

The upper 93 m of the borehole at Lade consist of Lower Ordovician greenstones while the lower part is characterised by trondhjemite based on driller's observations and an investigation with an optical televiewer. The borehole was tested for hydraulically active fractures with the help of a groundwater pump installed at 20 m depth. During pumping of water with a volumetric flow rate of 780 l hr^{-1}, a propeller was lowered in the borehole. The number of rounds per time interval can be used to detect and calculate groundwater flow through open fractures. In the depth around 34 m a pronounced fracture appears, which is visible in the flow measurement (reduction of number of rotations below 34 m) as well as in an optical televiewer image (see Figure 7). The televiewer image and the test data were made available by Harald Elvebakk who performed the measurements in 2003.

The effective thermal conductivity measured with the TRT is 4.11 W $m^{-1}K^{-1}$. This value is higher than the median rock core thermal conductivity measured in Norwegian greenstones (2.7 W $m^{-1}K^{-1}$, n=37, unpublished data, NGU) and trondhjemites (2.7 W $m^{-1}K^{-1}$, n=11, unpublished data, NGU).

The temperature profile at Lade is characterised by a negligible geothermal gradient and little variation along the borehole. However, the effective thermal conductivity measured at the borehole was higher than the laboratory measured thermal conductivities would suggest for greenstones and trondhjemites. A closer look at the temperature profile taken after the TRT reveals a faster recovery around 34 m than at the rest of the borehole (Figure 3).

As described above, the flow measurement showed a water-bearing fracture at this depth. A natural, regional groundwater flow can therefore be expected, similar as in the study of Liebel et al. (2011), which is responsible for an increased effective thermal conductivity. Even if the effect of the open fracture is rather small at Lade, it was chosen as an example because of the complete dataset comprising hydrogeological data for the borehole. A more pronounced effect of groundwater on the temperature profile than in this case can frequently be found (see e.g., Liebel et al. 2009).

Bjørnegård

The borehole at Bjørnegård (Bærum municipality, Oslo region) is drilled primarily in Ordovician limestones and shales according to the geological map and to outcrops from the area. The sedimentary cover is 28 m thick and consists of clays. The median thermal conductivity from rock core samples from the Ordovician limestones and shales is 2.7 W $m^{-1}K^{-1}$ (GEOS database, NGU 2011 unpubl.). The TRT result shows a pronounced higher effective thermal conductivity of 4.81 W $m^{-1}K^{-1}$. The driller's report indicates a water-bearing fracture at 60 to 62 m depth with a water yield of more than 1000 l hr^{-1}. The driller's estimate of the water yield for the entire borehole is 15000 l hr^{-1}. During drilling the borehole was artesian. After the drilling was finished, a tight plug was installed to stop the outflow from the borehole.

The temperature profiles at Bjørnegård show an anomalous temperature increase towards the surface (uppermost 10 m) which can be explained with two neighbouring injection wells where surface water is infiltrated into the aquifer with a total rate of ca. 38 litres per minute. Infiltration is done to avoid surface subsidence damages related to a lowered groundwater level as a consequence of the relatively new railway tunnel nearby. Figure 8 visually shows the hydrogeological situation at Bjørnegård.

The temperature profiles were taken in August 2010. The shallowest temperature field is altered due to solar irradiation on the parking lot and heat flow from the surface towards the ground (Figure 3). Elsewhere, the temperature profile before the TRT shows no unexpected variations. Very different, however, is the temperature profile after the TRT. The borehole cuts an open fracture at 60 m depth belonging to a presumably confined aquifer (artesian). Water intrudes the borehole and flows upwards to the next possibility where it can flow into the sur-

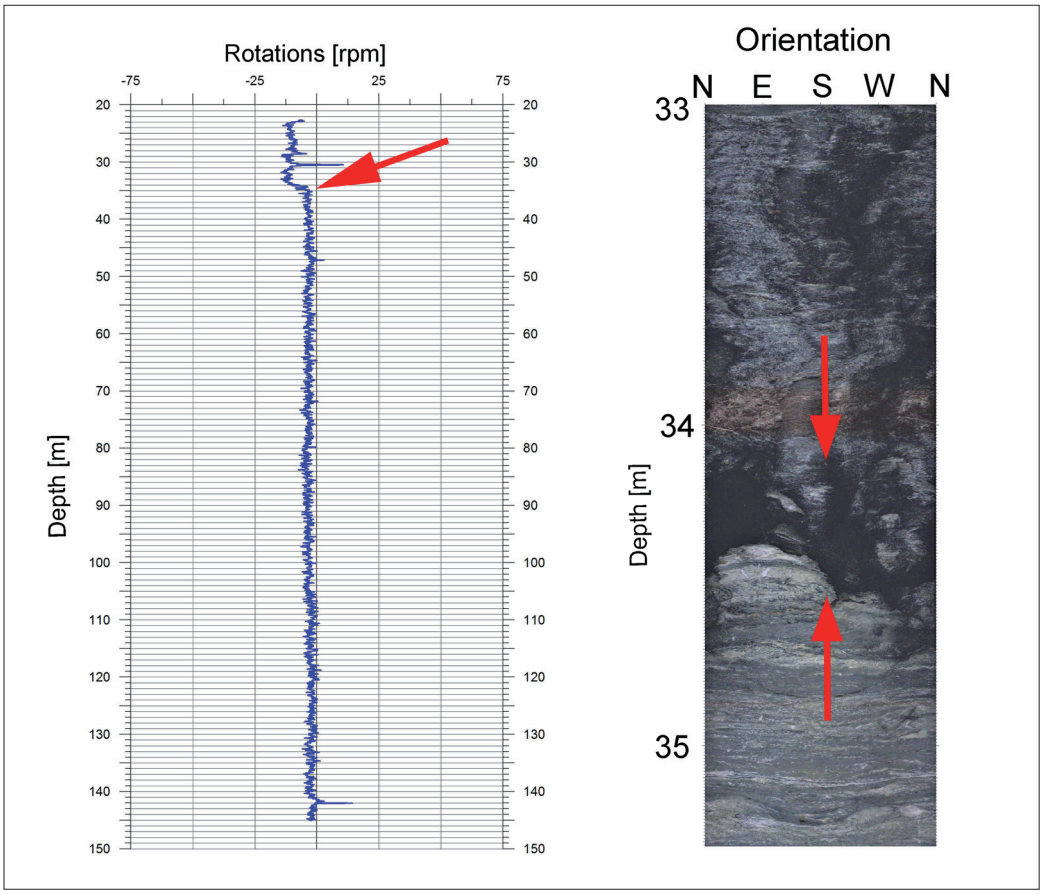

Figure 7. Results from the flow measurement (left) and optical televiewer image of the main fracture in the investigation borehole (right, H. Elvebakk, unpubl.); red arrows indicate the main fracture.

rounding formation, which is in this case at the contact between the bedrock and the sedimentary cover at about 28 m depth. Therefore, the temperatures recover fastest in the profile taken after the TRT in the interval between 60 and 28 m, while the heat takes longer to be dissipated in the other parts of the borehole. Similar temperature profiles were reported from Sweden (G. Hellström, pers. comm. 2011) and Germany (M. Sauer, pers. comm. 2011).

Conceptual models

Conceptual models of the four discussed cases are shown in Figure 9 and discussed in the following.

Case 1:

If the rocks in a borehole are homogeneous concerning mineral content and if no permeable fractures occur, a temperature profile may be measured after a TRT as shown in Figure 9. The temperature recovery after the TRT is fastest in the upper part of the borehole as the temperatures of the surrounding rocks are colder. Here the temperature gradient is largest resulting in a high heat flux according to Fourier's law. Further down in the borehole the undisturbed rock temperature increases according to a geothermal gradient. The temperature difference decreases between the heated borehole and the surrounding rock. Therefore, the temperature recovery is slow in the low part of the borehole (low heat flux). A temperature drop at the base of the borehole can be observed due to heat dissemination also in vertical direction.

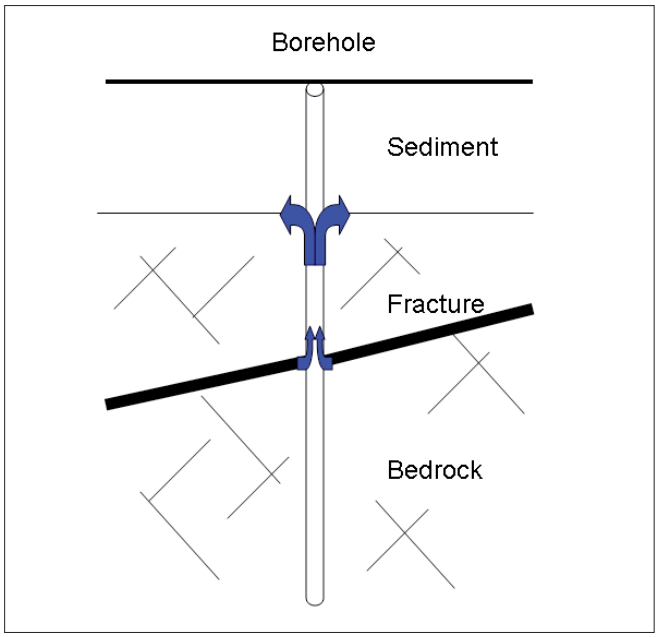

Figure 8. Schematic diagram showing the groundwater flow through the open fracture at Bjørnegård and the upward flow through the borehole with the final inflow into the sediments.

A temperature profile of this kind is the optimum for the TRT evaluation. The assumptions for the TRT analysis for example with the infinite line-source theory are met.

Case 2:
In case 2 the geological conditions are similar as in case 1 but the temperature in the upper part of the well is higher due to an increase in heat flow from the surface. Possible alterations may be due to the construction of a building with poor insulation towards the ground, a parking lot (pronounced effect with dark asphalt) or a forest clearing which increases the irradiation and the heat transfer towards the ground.

A temperature profile of this type does not implicate a special TRT evaluation. However, it gives valuable information on the expected operation of a ground-coupled heat pump installation. An increased heat transfer from the surface is positive for the heat extraction from the ground as the removed heat is restored fast from the surface.

Case 3:
If the borehole passes through a water-bearing fracture, a fast temperature recovery can be expected in the vicinity of the fracture (Figure 9).

If a temperature profile taken some hours after a TRT indicates a water-bearing fracture, the TRT results need a cautious interpretation. Groundwater flow through the borehole during the TRT can be discovered from the TRT results in certain circumstances. One possibility is that the effective thermal conductivity does not converge with time but does increase continuously (Witte 2002, 2007). If the groundwater flow volume through the open fracture is relatively small or if the total time of the TRT is chosen too short, this effect cannot be discovered

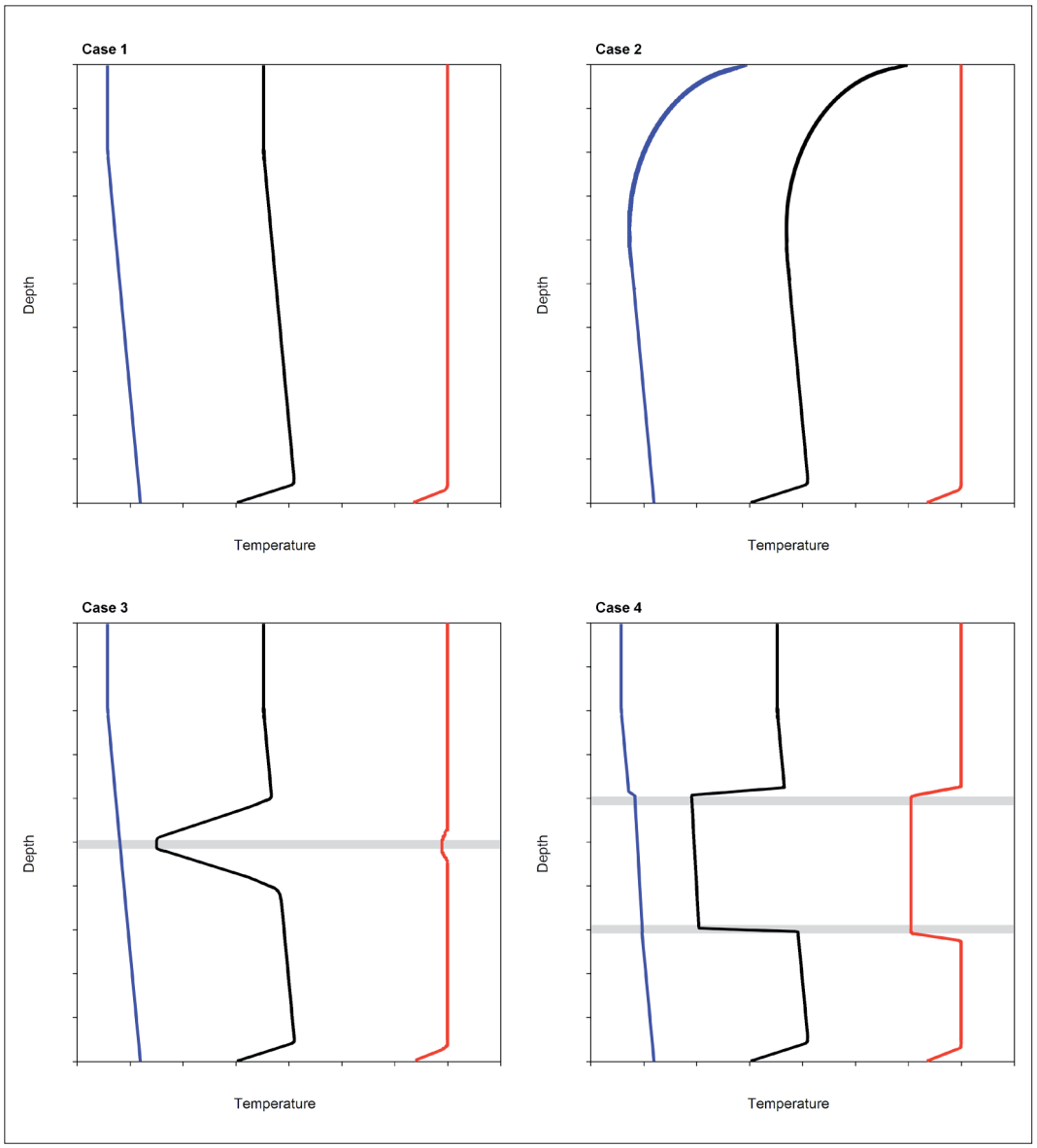

Figure 9. Fictitious temperature profiles before (blue), right after (red) and five hours after (black) a TRT in homogeneous rock for the four cases. Case 1: no water-bearing fractures; case 2: temperature anomaly towards the surface due to poorly insulated buildings or solar collectors (e.g., parking lot, pitch); case 3: one water-bearing fracture; case 4: two open fractures short-circuiting a confined lower aquifer with an unconfined upper aquifer.

in the TRT results. Results from a study in Bryn (Oslo region) show, however, that the effective thermal conductivity increased by 0.4 W $m^{-1}K^{-1}$ due to an increased groundwater flow through one fracture. In this case two TRTs were compared to each other, one without artificial groundwater flow and one with pumping of groundwater from a close-by well (for more details see Liebel et al. 2009).

Even if the groundwater flow is not detectable directly in the TRT results, it will transport heat away from the well during operation in cooling mode and it will transport heat towards the well in heating mode, which has to be taken into account for the dimensioning of a ground-coupled heat pump system.

The temperature profile after the TRT may indicate groundwater flow, even if the TRT results seem normal. In this case a more detailed hydrogeological investigation and a groundwater flow simulation should be performed to estimate the influence of groundwater on the borehole heat exchanger during operation. Parameter estimation techniques are a possibility to estimate the thermal conductivity based on the TRT results (e.g., Hellström 1997, Spitler et al. 1999).

A second explanation for a temperature profile with a fast recovery in one zone is a layer of improved thermal conductivity due to a different mineral content (for example a high quartz content). In most cases, the driller's observations of the colour of the drilling mud indicate different geological layers and mineral contents. If percussion drilling is applied, cuttings should be sampled in a regular interval (e.g., every three metres) to get more information about changing rock type and mineral content in the well. The driller's observations can be correlated to areas with fast temperature recovery in the temperature profile. In this case, the TRT results give effective thermal conductivities that converge and a standard data evaluation can be accomplished.

Case 4:
In this case the borehole penetrates two fractures where the lower one belongs to an artesian and the upper one to an unconfined aquifer. An upstream of groundwater towards the upper fracture is going to be established. Alternatively, the upper fracture can be replaced with the border between bedrock and permeable sedimentary cover.

A weaker upward flow might be established during the TRT if a thermosiphon effect appears (Gehlin et al. 2003).

The phenomenon of upwards flowing groundwater is easily discovered with the help of a temperature profile after the TRT as the temperature recovery will be fast in the area of flowing groundwater (Figure 9).

During a TRT, the temperature of the heat-carrier fluid in the borehole heat exchanger increases less if groundwater flow is present. The effect of upwards flowing groundwater on the effective thermal conductivity measurement may be stronger than of groundwater flow through fractures crossing the borehole. With up-flowing groundwater large areas of the borehole heat exchanger are affected by the contact with cold groundwater. In the case of horizontal fracture flow through the borehole, however, only limited areas of the borehole heat exchanger get in contact with cold groundwater. The measured effective thermal conductivity will be higher than the actual thermal conductivity of the bedrock in both cases, but highest in the case of upstreaming groundwater. Parameter estimation techniques are a possibility to estimate the thermal conductivity based on the TRT results (e.g., Hellström 1997, Spitler et al. 1999). For the dimensioning of a borehole field, further hydrogeological studies should be carried out, including a flow simulation for the influence area of the borehole field.

Conclusion

Temperature profiles before a TRT are taken as a standard procedure to calculate the undisturbed ground temperature and the thermal borehole resistance.

This study highlights the importance of taking temperature profiles also after the TRT is finished.

The temperature profiles yield important hydro- and thermogeological information based on a measurement that takes only about one hour. The driller's reports give an indication for areas of high probability for open fractures only. In the temperature profile after the TRT, the water-bearing fractures can be located precisely. Upcoming groundwater from confined artesian aquifers can be detected clearly. Layers of different mineral content showing varying thermal conductivities can be located and distinguished from zones of groundwater flow with the help of the driller's well reports.

Information gained from temperature profiles after a TRT, supplements the data obtained from various other sources such as: TRT, the driller's well report, rock core thermal conductivity measurements, the measurement of the undisturbed ground temperature, the geological map and so forth. The combined evaluation of all data available for a borehole can then be used to define the required capacity of a ground-coupled heat pump system and to predict the behaviour of the plant in operation. The extra information gained helps also to decide whether further site investigations or groundwater flow simulations are needed. Further work should focus on the quantification of the influence of groundwater flow on the estimate for the effective thermal conductivity.

Acknowledgements
We would like to thank the pre-submission readers and the reviewer of this manuscript (Bjarni R. Kristjànsson, NGI) for useful comments. The authors thank Båsum Boring AS for offering access to boreholes at Fredrikstad and Nordstrand and to AsplanViak for offering a borehole at Bjørnegård to be used for our scientific investigation. We are grateful to the Geological

Survey of Norway (NGU) for letting us use their TRT equipment and investigate their research borehole at Lade. Allan Krill (NTNU) corrected the English. The project was funded by the Norwegian University of Science and Technology (NTNU) and the Faculty of Engineering Science and Technology.

References

Acuña, J. and Palm, B. (2010) A novel borehole heat exchanger: Description and first distributed thermal response test measurements. Proceedings World Geothermal Congress 2010, Bali, Indonesia, 25–29 April 2010, 7 pp.

Andersson, O. (2011) Chapter 2 - Limitations. *In* McCorry, M. and Jones, G.L. (eds.) Geotrainet training manual for designers of shallow geothermal systems. Geotrainet, European Federation of Geologists, Brussels, pp. 15–20.

Austin, W.A. (1998) *Development of an in situ system for measuring ground thermal properties*. MSc thesis, Oklahoma State University, Stillwater, OK, USA, 164 pp.

Banks, D., Solbjørg, M.L. and Rohr-Torp, E. (1992a) Permeability of fracture zones in a Permian granite. *Quarterly Journal of Engineering Geology*, **25**, 377–388.

Banks, D., Rohr-Torp, E. and Skarphagen, H. (1992b) An integrated study of a Precambrian granite aquifer, Hvaler, Southeastern Norway. *Geological Survey of Norway, Bulletin*, **422**, 47–66.

Banks, D., Rohr-Torp, E. and Skarphagen, H. (1994) Groundwater resources in hard rock; experiences from the Hvaler study, southeastern Norway. *Applied Hydrogeology*, **94**, 33–42.

Clauser, C. and Huenges, E. (1995) Thermal conductivity of rocks and minerals. *In* Ahrens, T.J. (ed.) *Rock physics and phase relations–A handbook of pysical constants*. American Geophysical Union, Washington, USA, pp. 105–126.

Eskilson, P., Hellström, G., Claesson, J.,Blomberg, T. and Sanner, B. (2000) *Earth Energy Designer version 2.0*. Blocon software, Sweden.

Fujii, H., Okubo, H. and Chono, M. (2009) Application of optical fiber thermometers in thermal response tests for detailed geological descriptions. Proceedings of Effstock 2009 Conference on Thermal Energy Storage for Efficiency and Sustainability, Stockholm, Sweden, 6 pp.

Gehlin, S. (1998) Thermal response test. *In situ measurements of thermal properties in hard rock*. Licentiate thesis, Luleå University of Technology, 1998:37, 73 pp.

Gehlin, S. (2002) Thermal response test. *Method development and evaluation*. PhD thesis, Luleå University of Technology, 2002:39, 191 pp.

Gehlin, S.E.A. and Hellström, G. (2003) Influence on thermal response test by groundwater flow in vertical fractures in hard rock. *Renewable Energy*, **28**, 2221–2238.

Gehlin, S.E.A., Hellström, G. and Nordell, B. (2003) The influence of the thermosiphon effect on the thermal response test. *Renewable Energy*, **28**, 2239–2254.

Graversen, O. (1984) Geology and structural evolution of the Precambrian rocks of the Oslofjord-Øyeren area, southeast Norway. G*eological Survey of Norway Bulletin*, **398**, 1–49.

Gustafsson, A.M. (2006) *Thermal Response Test–Numerical simulations and analyses*. Licentiate thesis, Luleå University of Technology, 2006:14, 118 pp.

Gustafsson, A.M. and Westerlund, L. (2010) Multi-injection rate thermal response test in groundwater filled borehole heat exchanger. R*enewable Energy*, **35**, 1061–1070.

Gustafsson, A.M., Westerlund, L. and Hellström, G. (2010) CFD-modelling of natural convection in a groundwater-filled borehole heat exchanger. *Applied Thermal Engineering*, **30**, 683–691.

Hellström, G. (1997) Thermal response test of a heat store in clay at Linköping, Sweden. Proceedings of Megastock '97, Sapporo, Japan, pp. 115–120.

Holtedahl, O. (1953) *Norges geologi. Bind I*. Aschehoug & Co. Oslo, Norway, 583 pp.

Hughes, P.J. (2001) Geothermal heat pumps as a cost saving and capital renewal tool. E*nergy Engineering*, **98**, 59–80.

Ingersoll, L.R. (1948) *Heat conduction–With engineering and geological application*. McGraw-Hill Book Company, New York, USA, 278 pp.

Javed, S., Claesson, J. and Beier, R.A. (2011) Recovery times after thermal response tests on vertical borehole heat exchangers. Proceedings of The 23rd IIR International Congress of Refrigeration, Prague, Czech Republic, 9 pp.

Liebel, H.T., Huber, K., Frengstad, B.S., Ramstad, R.K. and Brattli, B. (2009) Thermogeology in the Oslo region and Kristiansand–Results from thermal response tests (TRT) with and without artificially induced groundwater flow. *NGU Report 2009.069*, 57 pp.

Liebel, H.T., Stølen, M.S., Frengstad, B.S., Ramstad, R.K. and Brattli, B. (2011) Insights into the reliability of different thermal conductivity measurement techniques: a thermo-geological study in Mære (Norway). *Bulletin of Engineering Geology and the Environment*, DOI: 10.1007/s10064-011–0394-3, 9 pp.

Lund, J.W., Freeston, D.H. and Boyd, T.L. (2005) World-wide direct use of geothermal energy 2005. Proceedings of World Geothermal Congress 2005, Antalya, Turkey, 20 pp.

Lund, J.W., Freeston, D.H. and Boyd, T.L. (2010) Direct utilization of geothermal energy 2010 worldwide review. Proceedings of World Geothermal Congress 2010, Bali, Indonesia, 23 pp.

Lutro, O. and Nordgulen, Ø. (2008) Oslofeltet, Bedrock geological map, scale 1:250,000, *Geological Survey of Norway*.

Nordell, B. (2008) Bergvärme och bergkyla–princip och funktion. Presentation at Informations- och utbildningsdagar, Föreningarna Byggnads och VVS-inspektörer, 8th of May 2008, Uppsala, Sweden.

Olesen, O., Dehls, J.F., Ebbing, J., Henriksen, H., Kihle, O. and Lundin, E. (2006) Aeromagnetic mapping of deep-weathered fracture zones in the Oslo Region–a new tool for improved planning of tunnels. *Norwegian Journal of Geology*, **87**, 253–267.

Pedersen, S. and Maaloe, S. (1990) The Iddefjord granite: geology and age. *Geological Survey of Norway Bulletin*, **417**, 55–64.

Philippe, M., Bernier, M. and Marchio D. (2009) Validity ranges of three analytical solutions to heat transfer in the vicinity of single boreholes. Geothermics, **38**, 407–413.

Roy, R.F., Blackwell, D.D. and Decker, E.R. (1972) Continental heat flow. Chapter 19. *In* Robertson, E.C. (ed.) *The Nature of the Solid Earth*, McGraw Hill, New York, USA, pp. 506–544.

Shonder, J.A. and Beck J.V. (1999) Determining effective soil formation properties from field data using a parameter estimations technique. *ASHRAE Transactions*, **105**, 458–466.

Signorelli, S., Bassetti, S., Pahud, D. and Kohl, T. (2007) Numerical evaluation of thermal response tests. *Geothermics*, 36, 141–166.

Slagstad, T., Balling, N., Elvebakk, H., Midttømme, K., Olesen, O., Olsen, L. and Pascal, C. (2009) Heat-flow measurements in Late Paleoproterozoic to Permian geological provinces in south and central Norway and a new heat-flow map of Fennoscandia and the Norwegian-Greenland Sea. T*ectonophysics*, **473**, 341–361.

Spitler, J.D., Yavuzturk, P.E.C. and Jain, N.K. (1999) Refinement and validation of in-situ parameter estimation models. Short report, Oklahoma State University, 6 pp.

Wagner, R. and Clauser, C. (2005) Evaluating thermal response tests using parameter estimation for thermal conductivity and thermal capacity. *Journal of Geophysics and Engineering*, **2**, 349–356.

Witte, H. (2002) Ground thermal conductivity testing: Effects of groundwater on the estimate. Abstract. 3. Kolloquium des Arbeitskreises Geothermik der DGG, Aachen, Germany, 1 pp.

Witte, H. (2007) Advances in Geothermal Response Testing. *In* Paksoy, H.Ö. (ed.) *Thermal Energy Storage for Sustainable Energy Consumption*, Springer, Netherlands, pp. 177–192.

Zervantonakis, I.K. and Reuss, M. (2006) Quality requirements of a thermal response test. Proceedings of the 10th International Conference on Thermal Energy Storage 'Ecostock 2006', Stockton, NJ, USA, 7 pp.

Age of the Hamningberg dolerite dyke, Varanger Peninsula, Finnmark: Devonian rather than Vendian – a revised interpretation

David Roberts

Geological Survey of Norway, P.O.Box 6315 Sluppen, 7491 Trondheim, Norway.
david.roberts@ngu.no

In an earlier geochronology paper in this same journal, discordant U–Pb ages on zircons from a dolerite dyke near Hamningberg, Varanger Peninsula, Finnmark, were interpreted to favour a Vendian (Ediacaran) age of intrusion for this dyke. A re-assessment of this interpretation, and further consideration of the field, geochemical and $^{40}Ar/^{39}Ar$ or K/Ar age characteristics that this dyke shares with other, unmetamorphosed, Devonian-age dolerite dykes in this same region of NE Norway and NW Russia, leads to the conclusion that the Hamningberg dolerite dyke is also most likely of Late Devonian age.

Introduction

In an attempt to date a prominent, 13.5 m-thick, mafic dyke located close to the former fishing settlement of Hamningberg in northeastern Varanger Peninsula, Finnmark, northern Norway (Figure 1), Roberts and Walker (1997) interpreted the U–Pb analyses on three discordant zircon fractions in favour of the given upper intercept age of 567.1 $^{+30}/_{-23}$ Ma and thus argued for a Late Vendian (Late Ediacaran)[1] age of emplacement for this particular dolerite dyke. The lower intercept of 392 $^{+25}/_{-36}$ Ma, on the other hand, was then considered to most likely represent a Late Devonian thermal overprint event.

Subsequently, in a geochemical study of dolerites and metadolerites from different areas in northernmost Finnmark, Rice et al. (2004) presented arguments that strongly favoured a Devonian age for the Hamningberg dyke, and concluded by asserting that *"the interpretation of the U–Pb age data [...] given by Roberts & Walker (1997) is rejected"*.

More recently, Herrevold et al. (2009) were sufficiently influenced both by the results of a $^{40}Ar/^{39}Ar$ study of mafic dykes on Varanger Peninsula (Guise and Roberts 2002) and by incisive comments raised by Dr. A.H.N. Rice in a manuscript review, to have followed Rice et al. (2004) in accepting the view that the Hamningberg dyke is likely to be of Late Devonian age.

Roberts, D. (2011) Age of the Hamningberg dolerite dyke, Varanger Peninsula, Finnmark: Devonian rather than Vendian – a revised interpretation. *Norges geologiske undersøkelse Bulletin*, **451**, 32–36.

The rebuttal of a Vendian (Ediacaran) age for this dyke, either directly or indirectly, by two different sources thus calls for a formal reply by the authors of the original U–Pb zircon investigation (Roberts and Walker 1997), and in the same NGU Bulletin journal. This is the main purpose of this short note, contributed in this case just by the first author as Dr. Walker unfortunately disappeared from the geoscience community in the USA almost ten years ago and has not been traced since.

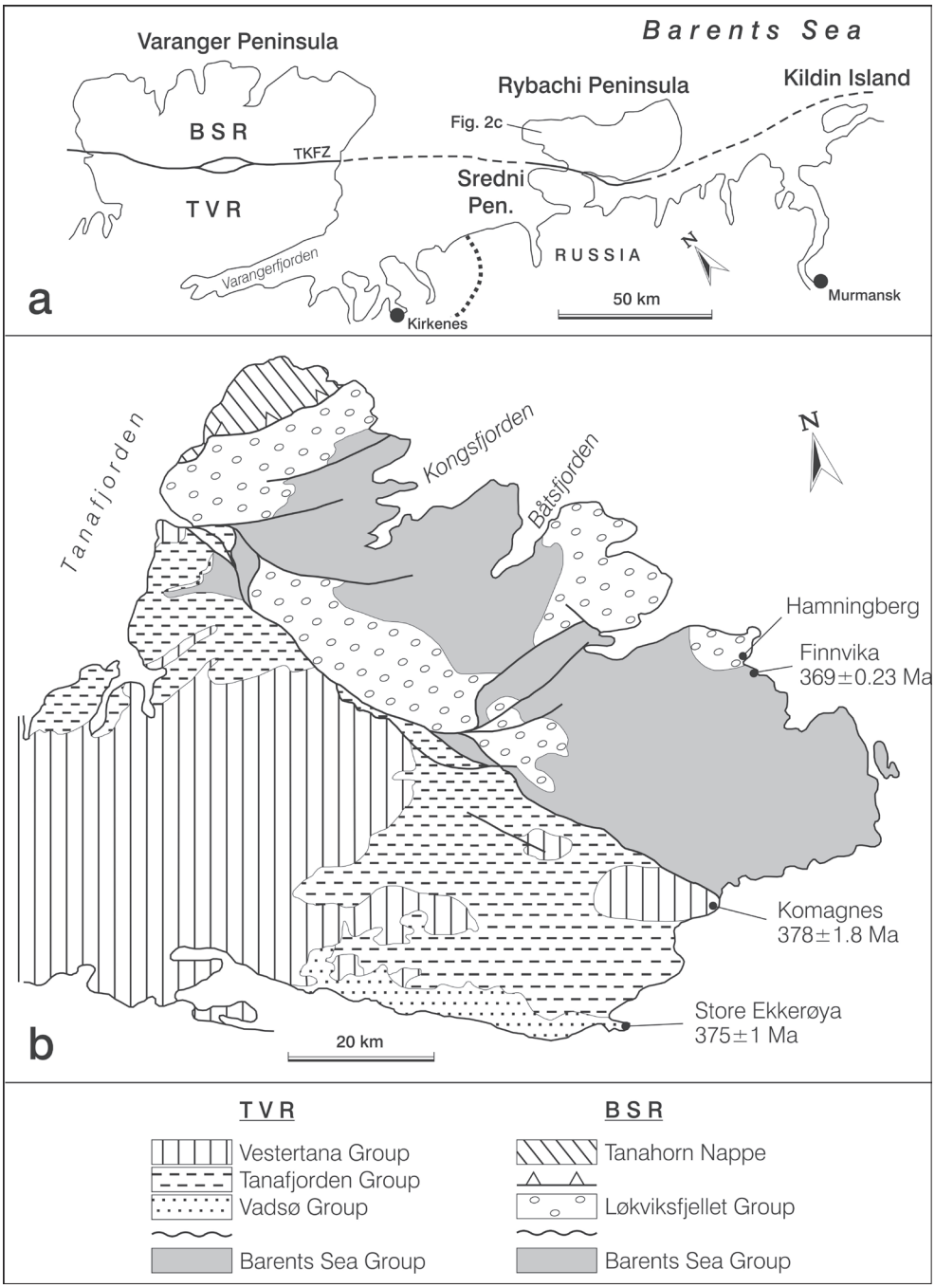

Figure 1. Simplified geological map of Varanger Peninsula (b) showing the location of the Hamningberg dolerite dyke. The locations of the Devonian dolerite dykes studied by Guise and Roberts (2002), at Finnvika, Komagnes and Store Ekkerøya, are also indicated. The outline map (a) shows the location of Rybachi Peninsula, Northwest Russia, and the dyke featured in Figure 2c. BSR–Barents Sea Region; TVR–Tanafjorden-Varangerfjorden Region; TKFZ–Trollfjorden-Komagelva Fault Zone.

[1] The term **Vendian**, introduced by Sokolov (1952) for the youngest period of the Neoproterozoic, has been, and still is, used in Russian and Nordic geological literature. In 2004, the IUGS International Commission on Stratigraphy decreed that the name Vendian should be replaced formally by **Ediacaran**, named after the Ediacara Hills in Australia where the soft-bodied Ediacara fossils were first discovered. However, the time ranges of the Vendian and Ediacaran are not identical. Whilst both terminate upwards at the base of the Cambrian, the base of the Vendian is taken at the base of the Smalfjord (Marinoan) tillite whereas the base of the Ediacaran is placed at the top of the Smalfjord Formation, just below a carbonate layer that caps the glacial deposit. Thus, the Ediacaran period is of shorter duration than the Vendian. In spite of losing its formality, the term Vendian is not invalid and can still be used as a legitimate chronostratigraphic unit.

Discussion

The ca NE–SW-trending, Hamningberg dolerite dyke cuts very low-grade sandstones of the Sandfjorden Formation of the Løkviksfjellet Group (Figures 1 and 2a), a siliciclastic succession of inferred Vendian/Ediacaran age which has been shown by Siedlecki and Levell (1978) to lie unconformably upon the Riphean to Lower Vendian Barents Sea Group (Vidal and Siedlecka 1983). Thin intercalations of shale in the sandstones carry a steep cleavage axial planar to regional N–S to NNW–SSE-trending folds. This cleavage, which is also cut by the dyke, has not yet been dated successfully, but work is in progress. Earlier, Taylor and Pickering (1981) produced an imprecise, Rb–Sr whole-rock, isochron age of 520 ± 47 Ma from cleaved mudstones near Hamningberg. Assessment of the regional geology, however, including neighbouring areas of NW Russia, has favoured a Late Vendian, Timanian age for the cleavage (Roberts 1995, Herrevold et al. 2009).

In their discussion, Roberts and Walker (1997) noted the moderate to strong discordance and scatter of the three fractions along the discordia line, and the fact that the large intercept uncertainties appear to relate to a combination of Pb loss and variable amounts of inheritance. Nevertheless, the authors chose to interpret the upper discordia intercept as indicating the approximate age of crystallisation of the dyke, i.e., ca. 567 Ma. Earlier, Beckinsale et al. (1975) had reported a K–Ar whole-rock age of 361 ± 10 Ma for the Hamningberg dyke; and a comparable, ca. NE–SW-trending, dolerite dyke near Finnvika (Figure 2b), just 3.5 km farther south, had yielded a K–Ar age of 363 ± 10 Ma. Both dykes had been reported to have almost identical geochemical signatures of continental within-plate type (Roberts 1975), a fact subsequently confirmed and elaborated upon by Rice et al. (2004).

In a $^{40}Ar/^{39}Ar$ study of plagioclase from three, geochemically similar, dolerite dykes from eastern Varanger Peninsula, Guise and Roberts (2002) reported comparable age spectra indicative of dyke emplacement at around 370 Ma, in latest Devonian (Famennian) time (Figure 1). These same dykes had earlier featured in the K–Ar work of Beckinsale et al. (1975), then also favouring a Late Devonian age of intrusion. Importantly, one of the three dykes investigated by Guise and Roberts (2002) was the Finnvika dyke. Thus, both the $^{40}Ar/^{39}Ar$ plagioclase and the K–Ar whole-rock dating studies had reached the same conclusion, which gave reason to question the interpreted Vendian, upper-intercept age for the nearby Hamningberg dyke.

As noted above, the analytical data presented by Roberts and Walker (1997) spread considerably along the discordia line and are not precisely colinear, a fact which led the authors to consider that there might be variable amounts of inherited zircon present in the zircon fractions. In such a case, the upper intercept age could represent an inheritance signature instead of a crystallisation age, and the lower intercept age of 392 $^{+25}/_{-36}$ Ma would then reflect the approximate age of dyke intrusion. Inheritance would most likely occur via magma contamination with assimilated country rocks – a suggestion forwarded by Rice et al. (2004). Thus, although the discordant zircon age results were originally interpreted as indicating a Vendian crystallisation age, the zircon data are also compatible with a Late Devonian age of intrusion for the dyke.

In the light of the accumulated body of evidence for other Devonian-age mafic dykes in the Varanger Peninsula and in other, adjacent areas of the Fennoscandian Shield, the Hamningberg dyke is now also considered to be Devonian. A feature of the few dolerite dykes in eastern Varanger Peninsula which are now reliably dated as Late Devonian is that they are unmetamorphosed, display pseudohexagonal to reticulate, columnar jointing and show distinctive orange-brown colours on weathered surfaces. In this regard, the Hamningberg dyke is no exception (Figure 2a). This 'trademark' for the Devonian dykes contrasts with the greenish-grey, schistose, metadolerite dykes (Figure 2e) of northwestern Varanger Peninsula (Roberts 1975) which have provided K–Ar and, in one case, Sm–Nd dating evidence of a Vendian/Ediacaran age (Beckinsale et al. 1975, Andersen and Sundvoll 1995, Rice et al. 2004). These metadolerites were clearly involved in Early Ordovician and later, less penetrative, Silurian orogenesis (Rice and Frank 2003).

Dolerite dykes occurring on Rybachi Peninsula in Russia (Figure 2c), some 60 km to the southeast of Varanger, trend NE–SW, and transect NW–SE-trending, Timanian (Vendian) folds and cleavage. They also show reticulate to pseudohexagonal jointing and display an orange-brown weathering crust (Roberts and Onstott 1995). In their $^{40}Ar/^{39}Ar$ study, Roberts and Onstott (1995) reported that isochron ages for three dykes range from ca. 402 to 376 Ma, but older model ages down to 450 Ma led them to cautiously interpret the dykes as being of possible Vendian to Cambrian age with a pervasive thermal overprint in Late Devonian time. In view of the field character of the unmetamorphosed Rybachi dykes, and their close resemblance to the Devonian dolerite dykes on Varanger Peninsula, also in terms of geochemistry, it is here considered more likely that they, too, are of Late Devonian age. In this same area of western Kola Peninsula, Pb–Zn vein mineralisations of Late Devonian age are commonly found in association with NE–SW- to N–S-trending dolerite dykes (Juve et al. 1995). The dolerite dykes were emplaced during a major episode of Mid to Late Devonian rifting, sedimentation and basaltic magmatism, associated with the Kontozero graben in this northern part of the Kola Peninsula and adjacent Barents Sea (Ziegler 1988, Bugge et al. 1995, Nikishin et al. 1996, Gudlaugsson et al. 1998, Drachev et al. 2010), a scenario which is also discussed in Guise and Roberts (2002). Many of the mafic dykes on Rybachi and other parts of Kola Peninsula were probably feeders to the basaltic lavas. Mafic dykes of comparable geochemistry occur farther southeast in the Devonian rift basins of the Timans where there are also thick accumulations of columnar-jointed basalts (Figure 2d).

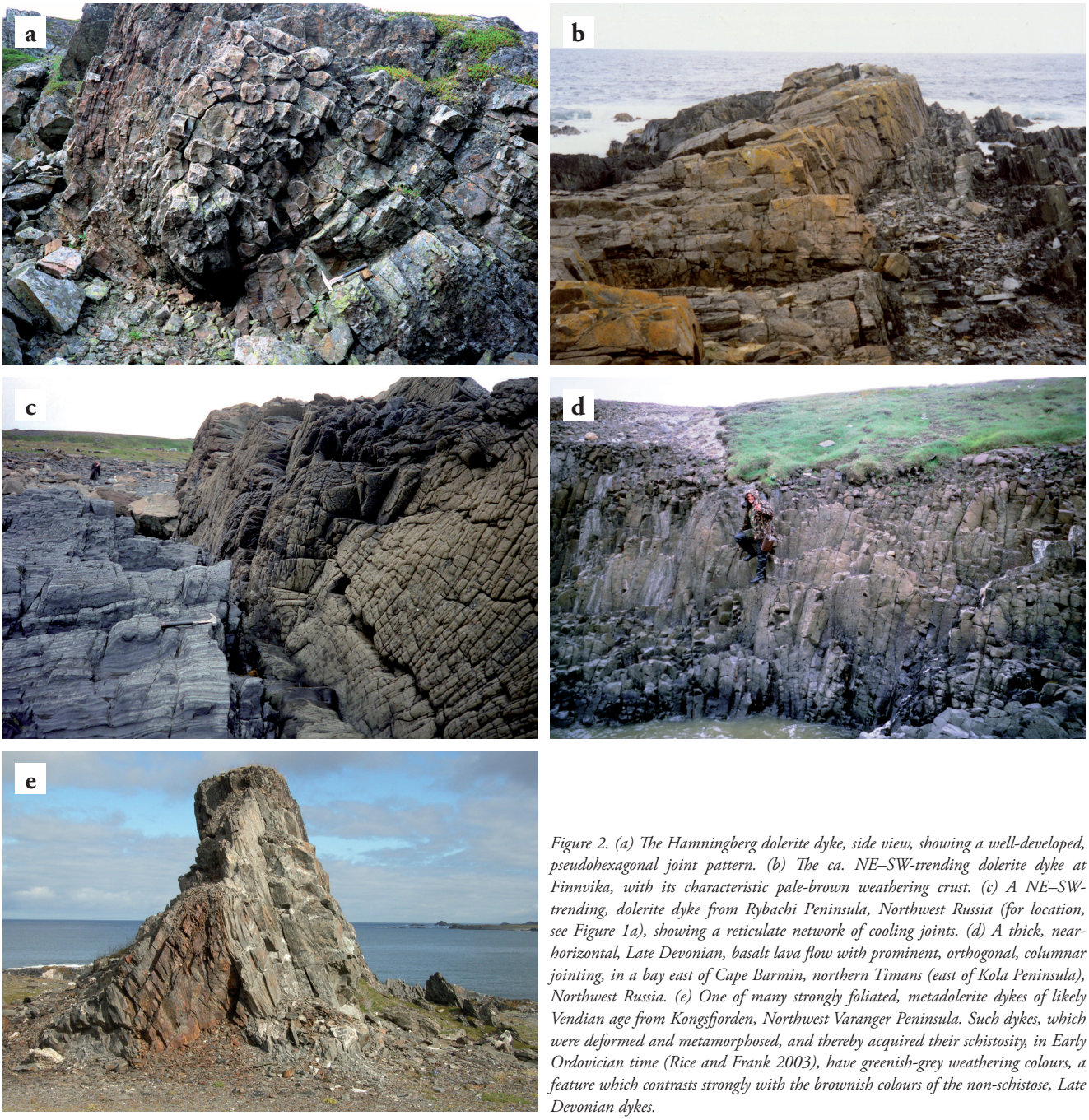

Figure 2. (a) The Hamningberg dolerite dyke, side view, showing a well-developed, pseudohexagonal joint pattern. (b) The ca. NE–SW-trending dolerite dyke at Finnvika, with its characteristic pale-brown weathering crust. (c) A NE–SW-trending, dolerite dyke from Rybachi Peninsula, Northwest Russia (for location, see Figure 1a), showing a reticulate network of cooling joints. (d) A thick, near-horizontal, Late Devonian, basalt lava flow with prominent, orthogonal, columnar jointing, in a bay east of Cape Barmin, northern Timans (east of Kola Peninsula), Northwest Russia. (e) One of many strongly foliated, metadolerite dykes of likely Vendian age from Kongsfjorden, Northwest Varanger Peninsula. Such dykes, which were deformed and metamorphosed, and thereby acquired their schistosity, in Early Ordovician time (Rice and Frank 2003), have greenish-grey weathering colours, a feature which contrasts strongly with the brownish colours of the non-schistose, Late Devonian dykes.

Acknowledgements

Discussions via e-mail with Peter Gromet and Hugh Rice on the mafic dykes and their age constraints, and on the U–Pb isotopic data and interpretation of discordia intercepts for the Hamningberg dyke in particular, are acknowledged with thanks. Professor Gromet read an early version of the typescript and offered helpful and perceptive suggestions which led to improvements in the final manuscript. Comments received from Stephen Lippard and a journal reviewer, Tore Herrevold, were also helpful in the final stages of typescript preparation.

References

Andersen, T. and Sundvoll, B. (1995) Neodymium isotopic systematic of the mantle beneath the Baltic Shield: evidence for depleted mantle evolution since the Archaean. *Lithos*, **35**, 235–243.

Beckinsale, R.D., Reading, H.G. and Rex, D.C. (1975) Potassium-argon ages for basic dykes from East Finnmark: stratigraphical and structural implications. *Scottish Journal of Geology*, **12**, 51–65.

Bugge, T., Mangerud, G., Elvebakk, G., Mørk, A., Nilsson, I., Fanavoll, S. and Vigran, J.O. (1995) The Upper Palaeozoic succession on the Finnmark Platform, Barents Sea. *Norsk Geologisk Tidsskrift*, **75**, 3–30.

Drachev, S.S., Malyshev, N.A. and Nikishin, A.M. (2010) tectonic history and petroleum geology of the Russian Arctic shelves: an overview. *In* Vining, B.A. and Pickering, S.C. (eds.) *Petroleum geology: from mature basins to new frontiers*. Proceedings of the 7th Petroleum Geology Conference, Geological Society, London, pp. 591–619.

Gudlaugsson, S.T., Faleide, J.I., Johansen, S.E. and Breivik, A.J. (1998) Late Palaeozoic structural development of the southwestern Barents Sea. *Marine and Petroleum Geology*, **15**, 73–102.

Guise, P.G. and Roberts, D. (2002) Devonian ages from $^{40}Ar/^{39}Ar$ dating of plagioclase in dolerite dykes, eastern Varanger Peninsula, North Norway. *Norges geologiske undersøkelse Bulletin*, **440**, 27–37.

Herrevold, T., Gabrielsen, R.H. and Roberts, D. (2009) Structural geology of the southeastern part of the Trollfjorden-Komagelva Fault Zone, Varanger Peninsula, Finnmark, North Norway. *Norwegian Journal of Geology*, **89**, 305–325.

Juve, G., Størseth, L.R., Vetrin, V.R. and Nilsson, L.P. (1995) Mineral deposits of the international 1:250,000 map-sheet Kirkenes. (Extended abstract) *Norges geologiske undersøkelse Special Publication*, **7**, 375–378.

Nikishin, A.M., Ziegler, P.A., Stephenson, R.A., Cloetingh, S.S.P.L., Furne, A.V., Fokin, P.A., Ershov, A.V., Bolotov, S.N., Korotaev, M.V., Alekseev, A.S., Gorbachev, V.I., Shipilov, E.V., Lankreijer, A., Bembinova, E.Y. and Shalimov, I.V. (1996) Late Precambrian to Triassic history of the East European craton: dynamics of sedimentary basin evolution. *Tectonophysics*, **268**, 23–63.

Rice, A.H.N. and Frank, W. (2003) The early Caledonian (Finnmarkian) event reassessed in Finnmark: $^{40}Ar/^{39}Ar$ cleavage age data from NW Varangerhalvøya, N. Norway. *Tectonophysics*, **374**, 219–236.

Rice, A.H.N., Ntaflos, T., Gayer, R.A. and Beckinsale, R.D. (2004) Metadolerite geochronology and dolerite geochemistry from East Finnmark, northern Scandinavian Caledonides. *Geological Magazine*, **141**, 301–318.

Roberts, D. (1975) Geochemistry of dolerite and metadolerite dykes from Varanger Peninsula, Finnmark, North Norway. *Norges geologiske undersøkelse*, **322**, 55–72.

Roberts, D. (1995) Principal features of the structural geology of Rybachi and Sredni Peninsulas, and some comparisons with Varanger Peninsula. *Norges geologiske undersøkelse Special Publication*, **7**, 247–258.

Roberts, D. and Onstott, T.C. (1995) $^{40}Ar/^{39}Ar$ laser microprobe analyses and geochemistry of dolerite dykes from the Rybachi and Sredni Peninsulas, NW Kola, Russia. *Norges geologiske undersøkelse Special Publication*, **7**, 307–314.

Roberts, D. and Walker, N. (1997) U–Pb zircon age of a dolerite dyke from near Hamningberg, Varanger Peninsula, North Norway, and its regional significance. *Norges geologiske undersøkelse Bulletin*, **432**, 95–102.

Siedlecki, S. and Levell, B.K. (1978) Lithostratigraphy of the Late Precambrian Løkvikfjell Group on Varanger Peninsula, East Finnmark, North Norway. *Norges geologiske undersøkelse*, **343**, 73–85.

Sokolov, B.M. (1952) On the age of the old sedimentary cover on the Russian Platform. *Izvestiya Akademii Nauk SSSR, Seriya eologicheskaya*, **5**, 21–31.

Taylor, P.N. and Pickering, K.T. (1981) Rb–Sr isotopic age determination on the Late Precambrian Kongsfjord Formation, and the timing of compressional deformation in the Barents Sea Group, East Finnmark. *Norges geologiske undersøkelse*, **367**, 105–110.

Vidal, G. and Siedlecka, A. (1983) Planktonic, acid-resistant microfossils from the Upper Proterozoic strata of the Barents Sea Region of Varanger Peninsula, East Finnmark, northern Norway. *Norges geologiske undersøkelse*, **382**, 145–179.

Ziegler, P.A. (1988) Evolution of the Arctic-North Atlantic and the Western Tethys. *American Association of Petroleum Geologists Memoir*, **43**, 198 pp.